SCIENCE CHINA
Chemistry

•REVIEWS•

December 2022 Vol.65 No.12: 2417–2436
https://doi.org/10.1007/s11426-022-1329-5

Electrochemiluminescence biosensing and bioimaging with nanomaterials as emitters

Yaqiang Feng[1], Ningning Wang[2,3] & Huangxian Ju[2*]

[1]*Research Center of Analytical Instrumentation, Key Laboratory of Synthetic and Natural Functional Molecule Chemistry of Ministry of Education, College of Chemistry and Materials Science, Northwest University, Xi'an 710127, China;*
[2]*State Key Laboratory of Analytical Chemistry for Life Science, School of Chemistry and Chemical Engineering, Nanjing University, Nanjing 210023, China;*
[3]*School of Pharmacy, Shandong Technology Innovation Center of Molecular Targeting and Intelligent Diagnosis and Treatment, Binzhou Medical University, Yantai 264003, China*

Received May 29, 2022; accepted July 6, 2022; published online October 8, 2022

The continuous emergence of novel luminophores has been leading the development of electrochemiluminescence (ECL) analysis since the ECL phenomenon of silicon nanoparticles was first reported in 2002. Nanomaterial-based luminophores termed as nanoemitters exhibit great application potential in ECL bioanalysis. In this review, we systematically summarize the research progress of various types of ECL nanoemitters, such as semiconductor quantum dots (QDs), carbon dots (CDs), polymer dots (Pdots), aggregation-induced emission nanoparticles (AIE dots), and other nanoemitters including luminophor-edoped silica nanoparticles, metal-organic frameworks, covalent organic frameworks, and metal nanoclusters. We mainly emphasize the characteristic of these nanoemitters and their applications in ECL biosensing and bioimaging by using them as labels, and highlight some impressive cases in the last five years. Finally, we discuss current challenges in the field of ECL nanoemitters and point out their prospects.

electrochemiluminescence, nanoemitters, biosensing, bioimaging

Citation: Feng Y, Wang N, Ju H. Electrochemiluminescence biosensing and bioimaging with nanomaterials as emitters. *Sci China Chem*, 2022, 65: 2417–2436, https://doi.org/10.1007/s11426-022-1329-5

1 Introduction

Electrochemiluminescence or electrogenerated chemiluminescence (ECL) is a light-emitting process, in which the excited state species (R^*) are generated *via* exergonic electron transfer on the working electrode, following the radiative transitions to the ground state [1,2]. As an analytical technique that combines electrochemical excitation and the detection of ECL intensity or sometimes ECL emission wavelength, ECL is electrochemically controllable, and the excited states can be produced without the need of extra light source, which endows this technique high selectivity with near zero-background, excellent precision, wide dynamic range, low sample consumption and rapid response time. Thus, ECL technology has been widely used in clinical diagnostics for the analysis of different disease biomarkers [3–10].

From the perspective of the development history of the ECL field, the exploitation and application of ECL luminophores are critical in promoting the continuous development of the ECL field. As early as 1927 and 1929, the ECL phenomena of Grignard reagent and luminol were discovered. Thereafter, the ECL properties and mechanisms of polycyclic aromatic hydrocarbons (PAHs) and metal complexes

*Corresponding author (email: hxju@nju.edu.cn)

were proposed, which led to the ECL theory of radical ion annihilation and coreactant pathways. In particular, the finding of $Ru(bpy)_3^{2+}$ as ECL emitter in 1972 and the occurrence of aqueous $Ru(bpy)_3^{2+}$-TPrA (tri-*n*-propylamine) ECL system in 1987 promoted the quick development of ECL fields. Now $Ru(bpy)_3^{2+}$ has been widely used in food, environmental and clinical testing. Up to now, a large number of review papers have summarized the ECL mechanisms and their analytical applications [11–18].

However, the small molecule luminophores often face the problems of insufficient signal intensity, difficult labeling, and high cost when applied to detection, which largely limits their application. Fortunately, nanomaterials have been exploited and applied as a novel class of ECL emitters (designated as nanoemitters) [19–21]. Their surface effects, quantum size effect, macroscopic quantum tunneling effect and quantum confinement effect endow the nanomaterials with unique and excellent ECL performance [22,23]. Compared with traditional molecular emitters, such as $Ru(bpy)_3^{2+}$ and luminol, nanoemitters are not only rich in active sites on nanoparticle surface and easy to modify, but also more controllable in ECL properties through changing the composition or size. More importantly, nanoemitters can also be used as ECL probes for biosensing and imaging due to their easy surface functionalization and more active centers in individual nanoparticle, which endows bioassay with higher sensitivity and better imaging capabilities.

In recent years, great progress has been made in applying ECL nanoemitters for biosensing and bioimaging. By using the change of ECL intensity upon molecular recognition as detection signal, the proposed biosensing and bioimaging methods have been used for highly specific analysis of small biomolecules, proteins, nucleic acids, *etc*. To improve the detection sensitivity, some nanomaterials have been employed for signal amplification through accelerating the electron transfer, their catalytic and enzyme mimetic functions, as the carriers of enzyme or signal molecules, or selective concentration of target biomolecules on nanomaterials [24,25]. As an emerging imaging technique, ECL imaging can collect electrochemical signal and optical image simultaneously, giving full use of the advantages of ECL temporal and spatial resolution, and has been widely used in multi-target analysis, visual detection and microscopic imaging. With the use of electron-multiplying charge-coupled device (EM-CCD) for ECL imaging, the detection of single object, including single particles, cells and biomolecules, has been achieved for revealing local biological and catalytic events with high spatiotemporal resolution [26].

In this review, we first systematically summarize the research progress of various types of ECL nanoemitters. We mainly emphasize the use of these nanoemitters in ECL biosensing and bioimaging, and highlight some impressive cases in the last five years (2018–2022). Finally, we discuss current challenges in the field of ECL nanoemitters, and point out their prospects.

2 Overview on ECL nanoemitters

Silicon quantum dot (QD) was the first reported nanoemitter, whose ECL could be produced *via* annihilation or coreactant pathway in organic solvents [27]. This pioneering work showed that QDs could successively store charge in solution, which led to light emitting behavior upon electron and/or hole transfer reactions. Afterward, ECL nanoemitters have expanded from the initial QDs [21] to other nanomaterials with different compositions and morphologies, including small molecule luminophores-doped silica nanoparticles (DSNPs) [28], metal clusters [29], organic small molecule nanoparticles [30], carbon-based nanomaterials [31], up-converting nanocrystal [32], two-dimensional nanomaterials [33], perovskite nanocrystals [34], semiconducting polymer dots (Pdots) [35], and aggregation-induced electrochemiluminescence (AIE) active nanomaterials [36,37] (Figure 1). As seen from the timeline of ECL nanoemitters, early studies of nanoemitters were mostly performed by measuring the ECL signal in organic solutions, such as acetonitrile or CH_2Cl_2 containing tetra-*n*-butylammonium perchlorate (TBAP) as a supporting electrolyte. To be suitable for biological applications, a large number of nanoemitters with good ECL emission in aqueous phase have been developed. These studies cover the fundamental ECL principles of nanoemitters and develop new signal switches and amplification strategies for bioanalysis. Therefore, the development of new ECL nanoemitters not only enriches the principle and system of ECL, but also promotes the development of ECL technology in bioanalysis.

The ECL of nanoemitters can be achieved through two pathways, the annihilation and coreactant pathway [23]. The annihilation pathway refers to the process of electrochemical reduction (injection of electrons) and oxidation (injection of holes) to generate anionic radicals ($R^{\bullet-}$) and cationic radicals ($R^{\bullet+}$) from nanoemitters, respectively, and then their collisional recombination forms excited states (R^*) and produces ECL emission. In the annihilation pathway, both anionic radicals and cationic radicals need to be obtained by electrochemical process. This pathway requires that the charged state of the nanoemitters must be sufficiently stable until an annihilation reaction occurs upon collision with an oppositely charged species. However, ECL emission cannot be obtained when the $R^{\bullet+}$ or $R^{\bullet-}$ of the nanoemitters are unstable, or the potential window of the solution is relatively narrow. To address these limitations, heterogeneous species, coreactants, are introduced into the electrolyte. Coreactants can produce highly redox-active intermediates upon oxidation or reduction, which can further react with nanoemitters

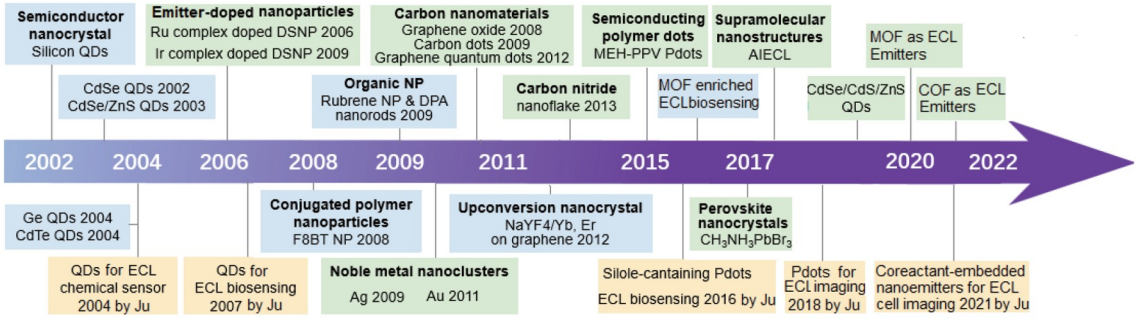

Figure 1 Time line of ECL nanoemitters. The blue shading box represents nanoemitters ECL generation from organic medium. The green shading box represents nanoemitter ECL generation in aqueous medium. The yellow shading box represents ECL application of nanoemitters (color online).

to produce ECL excited states. Unlike ECL from annihilation pathway, which requires the production of oxidized and reduced state emitters, coreactant pathway usually requires only a unidirectional potential sweep to generate ECL. Depending on the polarity of the applied potential, the ECL of the coreactant pathway can be further divided into "oxidative-reduction" and "reductive-oxidation" ECL. In the former, the coreactant undergoes electrochemical oxidation to form a highly reductive intermediate that reacts with the oxidized nanoemitter to produce anodic ECL (Figure 2a). The coreactants mainly include TPrA, oxalate, sulfite, and 2-(dibutylamino)ethanol. The latter undergoes the electrochemical reduction of the coreactant to form a highly oxidative intermediate that reacts with the reduced nanoemitter to produce a cathodic ECL (Figure 2b). Corresponding coreactants include peroxydisulfate ($S_2O_8^{2-}$) and hydrogen peroxide. Due to the participation of coreactants, the ECL efficiency or intensity is greatly improved, and thus modern ECL analyses are almost exclusively based on this pathway [22].

Nanoemitters can be divided into bulk phase (core) and surface domain. In the former metallic and non-metallic ions align periodically in long-range order, and the latter possesses an asymmetric chemical environment resulting from unpaired electrons, dangling bonds, ligand coordination, and crystalline defects. The two domains correspond to different electronic states and energy level distributions. According to this difference, the ECL emission of nanoemitters can be divided into the band-gap model and surface-state model for revealing the nature of excited states [23]. The surface-state of nanoemitters can produce a narrower surface energy level bandgap than that of the core due to the existence of surface defects [38], resulting in a red-shifted ECL spectrum relative to photoluminescence (PL) spectrum and a lower potential ECL emission (Figure 2c). The band-gap model is contributed by the core emission of nanoemitters [39], which usually has the same ECL emission spectrum as PL, size-dependent ECL behavior, and good monochromaticity (Figure 2d). Surface-state ECL is sensitive to the surface states of nanoemitters and can be used to probe the surface properties, while band-gap ECL has size-dependent effects and is well suited for multiplexing ECL analysis.

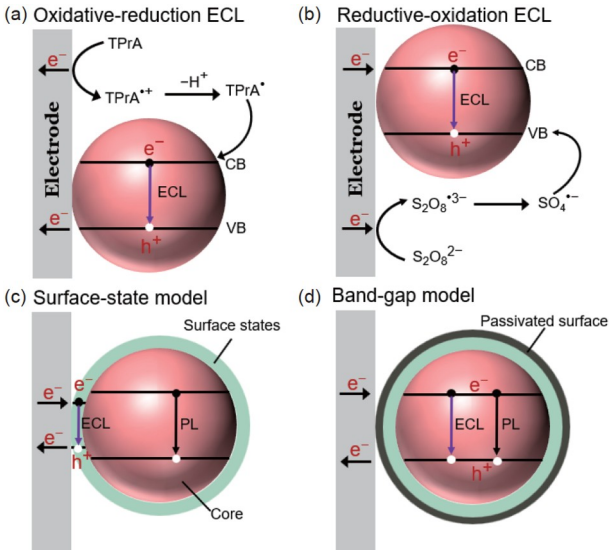

Figure 2 Simplified representation of coreactant ECL mechanism and emission model of nanoemitters. (a) Oxidative-reduction ECL with TPrA as a coreactant; (b) reductive-oxidation ECL with $S_2O_8^{2-}$ as a coreactant; (c) surface-state model; (d) band-gap model (color online).

Up to now, a variety of nanoemitters have been developed, with very different compositions, sizes and morphology. In terms of bioanalysis, good ECL nanoemitters should satisfy: (1) excellent ECL properties in aqueous media, mainly including high ECL efficiency, low excitation potential, and good ECL stability; (2) easy to biofunctionalize or label as a probe; (3) good biocompatibility, especially no cytotoxicity in living cells. Based on this criterion, we select the most promising ECL nanoemitters for review, including QDs, CDs, Pdots, and AIE dots. The comparison of their properties with $Ru(bpy)_3^{2+}$ is provided in Table 1. The application of these nanoemitters in ECL biosensing and bioimaging is progressing rapidly, especially in the detection of disease-related biomarkers, such as small biomolecules, proteins, nucleic acid, and cells.

Table 1 Comparison of the properties of nanoemitters with $Ru(bpy)_3^{2+}$ in aqueous media

Property	$Ru(bpy)_3^{2+}$	QDs	Carbon Ds	Pdots	AIE dots	DSNP
Structure	Molecular	Crystalline	Amorphous-crystalline	Amorphous	Amorphous	Amorphous
Water solubility	Good	Poor-moderate	Moderate	Poor-moderate	Poor-moderate	Moderate
Toxicity	High	High	Low	Low	Low	Moderate
Redox reversibility	Reversibility	Irreversibility	Irreversibility	Reversibility-irreversibility	Irreversibility	Reversibility
ECL emission	Anodic and cathodic	Anodic and cathodic	Anodic and cathodic	Anodic	Anodic	Anodic
Emission wavelength (nm)	610	Visible	Visible-NIR	Visible	Visible	Visible
Emission FWHM (nm)	60–80	20–200	30–200	50–100	50–200	60–80
ECL stability	High	Moderate	Poor	Poor	Poor	Moderate
ECL efficiency	1	Million times	Low	0.39–4 times	Several times	Several times
Multicolor	Difficulty	Easy	Difficulty	Easy	Difficulty	Difficulty
Biosensing application	Excellent	Good	Moderate	Moderate	Moderate	Moderate
Bioimaging application	Many	Few	No	Many	Few	Many

3 ECL of semiconductor QDs for biosensing

QDs are semiconductor nanocrystals with smaller sizes than the Bohr exciton diameter, exhibit size-dependent electrical and optical properties, and have been widely used in display, lighting, laser, solar energy harvesting, quantum information, optical sensing and bioimaging [40]. So far, various QDs have exploited their ECL activity in solution and in films ranging from elemental to compound semiconductor QDs [41], such as Si [27], Ge [42], CdS [43], CdSe [44], CdTe [45], PbS [46], CdSe/ZnSe [47], and CdSe/CdS/ZnS QDs [48]. The first ECL sensing application of QDs in aqueous solution was developed by Ju group in 2004 [49]. This work utilized the cathodic ECL signal of CdSe QDs to detect coreactant H_2O_2 based on the phenomenon that dissolved oxygen and hydrogen peroxide affect greatly the ECL intensity of QDs. H_2O_2 can participate in a variety of biological processes as a substrate of peroxidase, which lays the foundation for the construction of ECL biosensors. In 2007, the earliest QDs-based ECL biosensor was proposed for peroxidase-related analytes, such as glucose by incorporating glucose oxidase into CdSe QDs film [50]. Because biomolecules generally exist in aqueous systems, the synthesis of water-soluble QDs is the key to developing their bioanalytical applications. The first step in the ECL bioanalysis application of QDs is to transfer QDs from the organic phase to the aqueous phase. By utilizing different water-soluble surface ligands (thioglycolic acid, mercaptopropionic acid, and dimercaptosuccinic acid) to modify QDs (CdSe, CdS, CdTe), and combining with different signal amplification strategies, a variety of QDs-based ECL biosensors were constructed for nucleic acid analysis [51], immunoassay [52–55], cytosensing [56], and the detection of other biomolecules [57–60].

Developing low potential ECL systems is always strongly anticipated for ECL biosensing and bioimaging due to less inherent electrochemical interference and improved long-term stability of the biosensors. The existence of surface defects in unpassivated QDs, which can produce a narrower surface energy level bandgap than that of the core, results in a red-shifted ECL spectrum relative to PL spectrum and a lower potential ECL emission, as discussed above. Ju group [38] achieved the earliest low-potential ECL by using bidentate chelate as a stabilizer to form surface traps on the QDs. The dithiol compound-capped CdTe QDs exhibited a relatively low cathodic ECL emission at −0.85 V (*vs*. Ag/AgCl), which was used to construct ECL biosensor of hydroquinone based on the quenching effect of ECL emission of this QDs by consumption of coreactant H_2O_2. Recently, Zou group [61] investigated the ECL from $CuInS_2$@ZnS QDs on monodispersed state or surface-confined state with five different thiol capping agents, glutathione (GSH), thiosalicylic acid (TSA), *meso*-2,3-dimercaptosuccinic acid (DMSA), *N*-acetyl-*L*-cysteine (NAC), and *L*-homocysteine (HCY) (Figure 3A). They found that the ECL intensity and triggering potential of $CuInS_2$@ZnS QDs with different thiol capping agent were significantly different upon changing the luminophores from the monodispersed state to the surface-confined state. Moreover, by employing GSH as the capping agent of luminophores, the oxidative-reduction ECL of $CuInS_2$@ZnS-GSH/$N_2H_4{\cdot}H_2O$ not only exhibited the highest ECL intensity on surface-confined state but also demonstrated the lowest triggering potential around 0.32 V (*vs*. Ag/AgCl) for luminophores compared with other thiol capping agents, *i.e*., TSA (0.35 V), DMSA (0.36 V), NAC (0.44 V), HCY (0.37 V) (Figure 3B). Compared with PL spectrum (Figure 3C, curve a), the ECL spectrum of $CuInS_2$@ZnS-GSH exhibited a red-shifted ECL spectrum around 740 nm on surface-confined state (Figure 3C, curve c), almost identical to that for monodispersed state (Figure 3C, curve b), indicating that the surface of the $CuInS_2$@ZnS-GSH was not completely passivated. By immobilizing $CuInS_2$@ZnS-

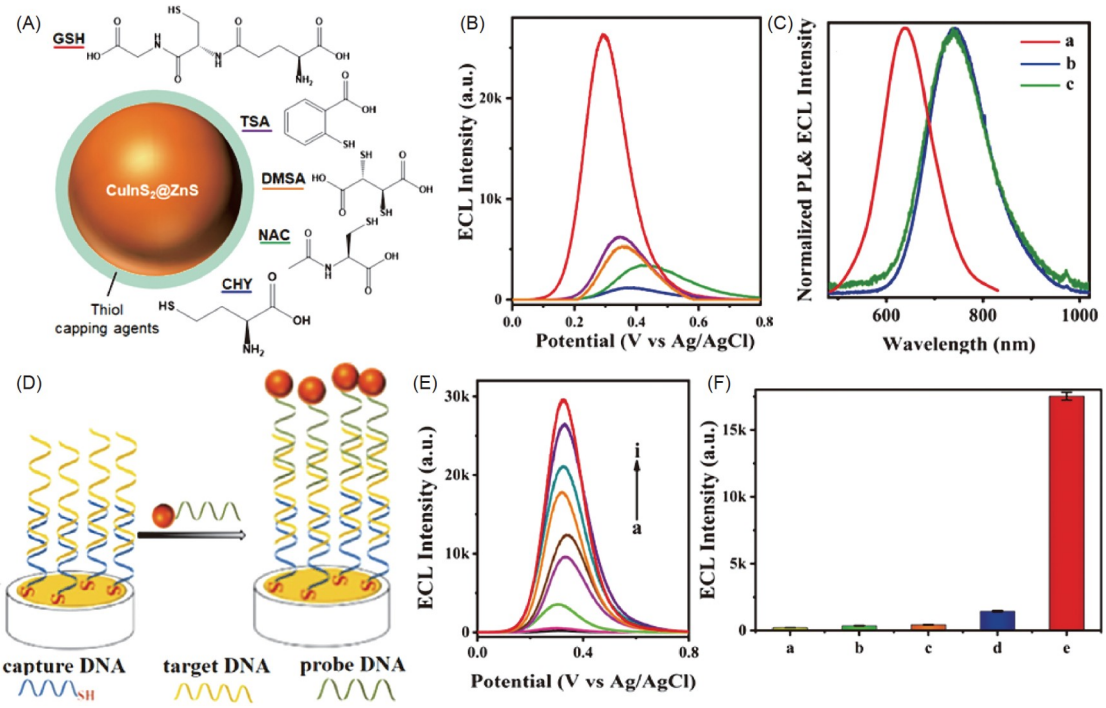

Figure 3 Surface-confined ECL of QDs for low-potential determining *KRAS* gene [61]. (A) $CuInS_2$@ZnS QDs with different thiol capping agents: glutathione (GSH), thiosalicylic acid (TSA), *meso*-2,3-dimercaptosuccinic acid (DMSA), *N*-acetyl-*L*-cysteine (NAC), and *L*-homocysteine (HCY). (B) Effects of thiol capping agent on the triggering potential of ECL from surface-confined state of $CuInS_2$@ZnS QDs with $N_2H_4{\cdot}H_2O$ as coreactant: GSH (red line), TSA (purple line), DMSA (orange line), NAC (green line), and CHY (blue line). (C) Normalized PL (a, red line) and ECL spectra of ZnS-GSH of the monodispersed state (b, blue line) and surface-confined state (c, green line). (D) Schematic illustration of the procedure for determining the *KRAS* gene with $CuInS_2$@ZnS-GSH QDs as ECL Tags by sandwich-type DNA hybridization. (E) ECL response of Au|capture DNA|target DNA|probe DNA| $CuInS_2$@ZnS-GSH QDs to samples containing (a) 0, (b) 0.5, (c) 1, (d) 5, (e) 10, (f) 50, (g) 100, (h) 500, and (i) 1,000 pM *KRAS* gene. (F) Specificity of Au| capture DNA|target DNA|probe DNA| $CuInS_2$@ZnS-GSH QDs to (a) blank sample and the samples containing (b) all-base mismatched DNA, (c) three-base mismatched DNA, (d) single-base mismatched DNA, and (e) target DNA of 50 pM. ECL measurements were conducted in 0.10 M pH 7.4 PB containing 100 mM KNO_3 and 20 mM $N_2H_4{\cdot}H_2O$ at 50 mV/s (color online).

GSH onto the Au electrode *via* Au–S bond and sandwich-type DNA hybridization, a surface-confined ECL sensor was proposed for sensitively and selectively determining the *KRAS* gene (Figure 3D). Under optimal conditions, the ECL response of Au|capture DNA|target DNA|probe DNA| $CuInS_2$@ZnS-GSH increased gradually along with the increase of *KRAS* gene concentration from 1 to 1,000 pM (Figure 3E). The signal was linearly related to the logarithm of *KRAS* gene concentration from 1 to 500 pM with a limit of detection (LOD) of 0.5 pM (signal-to-noise ratio of 3), and gave good specificity when the sample containing all-base mismatched DNA, three-base mismatched DNA, and single-base mismatched DNA (Figure 3F). This work demonstrated that the surface state of QDs and surface-confined strategy could be utilized to fabricate the low-triggering-potential ECL biosensor with acceptable selectivity and sensitivity.

Screening coreactant with low oxidative potential is also an important way to achieve the low-potential anodic ECL and their biosensing. Sulfate was firstly proposed as anodic coreactant of mercaptopropionic acid-modified CdTe QDs, which led to an oxidative-reduction ECL emission of QDs in aqueous solution at relatively low potential. By combining an enzymatic cycle of trace tyrosinase to produce the oxidized product with an energy-transfer process, an extremely sensitive ECL biosensor was developed for the detection of tyrosine with a subpicomolar LOD [59]. Recently, hydrazine hydrate was explored to act as an oxidative-reduction coreactant for achieving low-triggering-potential ECL from thiol-capped $CuInS_2$@ZnS QDs in aqueous medium [62,63]. With hydrazine hydrate as a coreactant, a potential-resolved anodic electrochemiluminescence multiplexing immunoassay was developed by utilizing water-soluble $CuInS_2$@ZnS QDs and $[Ru(bpy)_2(dcbpy)]^{2+}$ as luminophores. Hydrazine hydrate could be electrochemically oxidized to reduce radicals and then reacted with the electrochemically oxidized $CuInS_2$@ZnS QDs and $[Ru(bpy)_2(dcbpy)]^{2+}$ in sequence to produce coreactant ECL. The potential-resolved ECL of $CuInS_2$@ZnS QDs and $[Ru(bpy)_2(dcbpy)]^{2+}/N_2H_4$ could be well defined and distinguished from each other upon potential scanning and utilized for simultaneously determining human prostate specific antigen and carcinoma antigen 125 at the pathological cut-off concentration [64]. An environmentally-friendly coreactant, carbohydrazide, could be electrochemically oxidized at ~0.25 V *vs*. Ag/AgCl through the eight-electron releasing process, and the generated radicals

could reduce the luminophores for giving low potential ECL emission around 0.55 V under physiological conditions [65].

Multiplexing assay, which can detect multiple analytes simultaneously in a single assay, has long been seek in the ECL field [66–68]. QDs are particularly suitable for ECL multiplexing assays due to their size-tunable optical properties and narrow linewidth [69]. So far, QDs-based ECL multiplexing assays have been explored by two approaches, spectrum-resolved way [69] and potential-resolved way [70,71]. However, the poor monochromaticity of ECL from surface-sensitive QDs limits their application in this regard. Recently, Zou group [72] synthesized the dual-stabilizers-capped CdTe and CdSe QDs with monochromatic ECL emission and utilized them as ECL tags for simultaneously detecting two antigens. The dual-stabilizers, mercaptopropionic acid and sodium hexametaphosphate, were capped on QD surface for effectively removing the nonradiative surface state and deep surface trap of QDs for improving ECL efficiency and monochromaticity (Figure 4a) [39]. The dual-stabilizers-capped CdSe QDs showed a narrow ECL peak at ~550 nm, while the dual-stabilizers-capped CdTe QDs showed a nearly symmetrical and relatively broad ECL peak at ~776 nm. Due to the well spectrally distinguishable ECL emission from CdSe QDs (550 nm) and CdTe QDs (776 nm), a spectrum-resolved dual-color ECL immunoassay was constructed for the detection of carcinoembryonic antigen (CEA) and alpha fetoprotein (AFP) with an extremely LOD of 1 pg/mL and 10 fg/mL, respectively [72]. Recently, the same research group explored the spectrum-resolved triplex-color ECL multiplexing immunoassay using three dual-stabilizers-capped QDs as ECL tags (Figure 4b, c) [69]. The dual-stabilizers-capped CdSe550, CdTe650, and CdTe776 QDs showed nearly symmetrical and relatively narrow PL peaks around 550, 650, and 776 nm, respectively. These were consistent with the maximum wavelengths of ECL emission upon sandwich immunoreactions, indicating highly passivated surface-states in immune-complexes. The analysis results showed negligible cross-reactivity, high color-selectivity and excellent sensitivity for simultaneous detection of three antigens.

Although the above-mentioned highly passivated QDs exhibited good monochromaticity and narrow linewidths, their quantum yields were not high due to the possible introduction of a large number of electron and hole defects inside the lattice of QDs by aqueous phase synthesis, which seriously reduced the ECL efficiency of QDs and led to the red-shift and broadening of the ECL spectrum. Recently, Cao *et al*. [48] synthesized a water-soluble defect-free CdSe/CdS/ZnS core/shell/shell QDs that exhibited near-perfect ECL properties with highly efficient, stable and multicolor ECL.

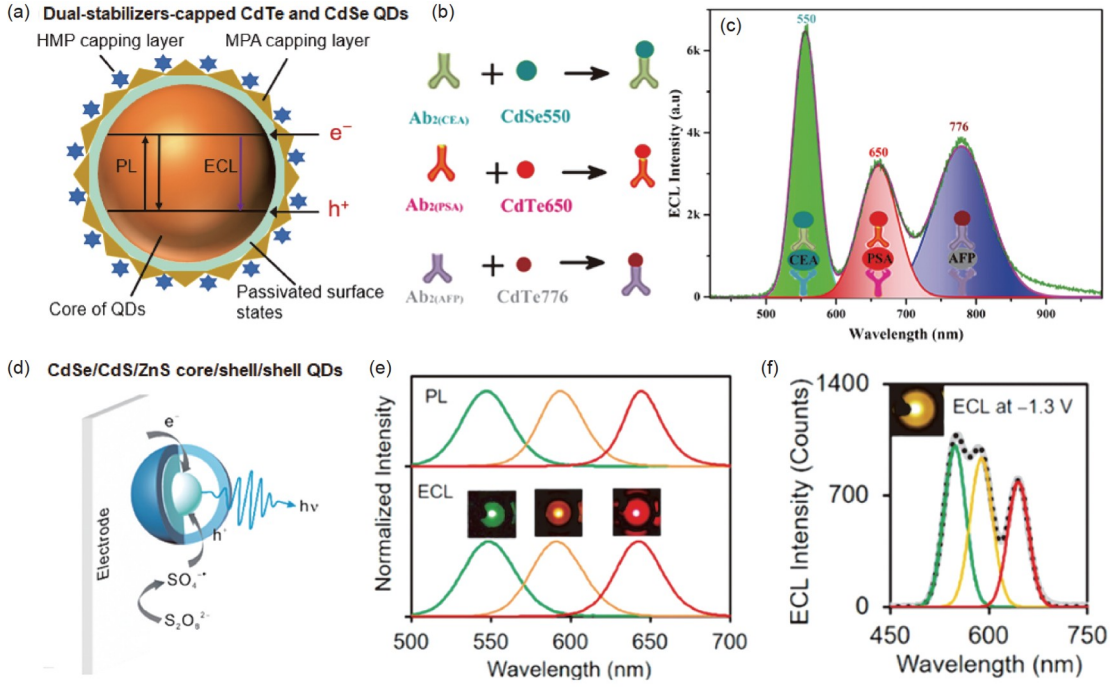

Figure 4 Monochromatic ECL generation from QDs for multiplexing immunoassay. (a) Monochromatic ECL from dual-stabilizers-capped CdTe and CdSe QDs. HMP, sodium hexametaphosphate. MPA, mercaptopropionic acid [39]. (b) Bioconjugation antibody with CdSe550, CdTe650, and CdTe776 QDs as ECL tags, and (c) spectrum-resolved triplex-color ECL multiplexing immunoassay *via* sandwich mode for simultaneous detection of 10 ng/mL CEA, 100 ng/mL PSA, and 100 pg/mL AFP [69]. (d) Schematic diagram of cathodic ECL generation from CdSe/CdS/ZnS core/shell/shell QDs with $S_2O_8^{2-}$ as coreactant, and (e) multicolor ECL generation from CdSe/CdS/ZnS core/shell/shell QDs with different core sizes. Normalized PL (top) and ECL spectra (bottom) of green-, yellow-, and red-emitting CdSe/CdS/ZnS core/shell/shell QDs. The middle inset shows the ECL photographs captured for different QDs. (f) ECL spectra and photographs (insets) of the ternary QDs mixture at excitation potential of −1.3 V [48] (color online).

The additional wide-bandgap ZnS outer shells were epitaxially grown on the CdSe/CdS core/shell QDs to isolate surface traps accessible for ECL generation (Figure 4d). This QD exhibited band-gap ECL emission due to its ECL spectrum nearly identical with PL spectrum (Figure 4e). The ECL efficiency in aqueous PBS was about six orders of magnitude higher than that of the standard $Ru(bpy)_3^{2+}$. The spectrum- and potential-resolved multicolor ECL generation from this QD could be achieved by controlling CdSe core with different sizes (Figure 4e, f). This bright ECL emitters with multicolor emission were ideal for high sensitivity and multiplexing biomedical detection and diagnosis.

As the earliest developed nanoemitters, the ECL from QDs shows fascinating application prospects in biosensing. By introducing surface defects on surface of QDs, low-potential ECL biosensing can be achieved. By surface passivation or engineering the interior inorganic structure of QDs, multicolor ECL emission can be achieved for multiplexing analytes simultaneously in a single assay. It should be noted that, in the application of QDs containing heavy metals such as Cd, Pb, and Hg, it is necessary to consider their toxicity, especially the problem of post-use treatment. Previous studies demonstrated that mercaptoacetic-stabilized CdSe QDs could release free Cd^{2+} into biological environment and cause cell death [73]. In addition, QDs could generate reactive oxygen species (ROS) to induce the toxicity, which can lead to organelle damage and cell death [74]. Therefore, the development of non-toxic QDs with excellent ECL properties is a future direction [71].

4 ECL of carbon dots for biosensing

Carbon dots (CDs) are a general term for nanoscale carbon-based nanomaterials with a characteristic size less than 10 nm. Compared with inorganic semiconductor quantum dots, these CDs have the advantages of low toxicity, good water solubility, easy functionalization, and inexpensive preparation. Based on the difference in shape, degree of crystallization and quantum confinement effects, CDs can be classified into graphene quantum dots (GQDs), carbon quantum dots (CQDs), carbon nanodots (CNDs), and carbonized polymer dots (CPDs) [75]. In addition, heteroatom-doped CDs are also an important category denoted with an addition prefix, such as nitrogen-doped CDs (N-CDs) [76]. As a prominent photoluminescent material, the photoluminescence mechanism of CDs is currently not fully understood and the proposed photoluminescence mechanisms include quantum confinement effect, defect states, molecular (fluorophore) states and crosslink-enhanced emission states [75]. The fluorescence properties of CDs and their applications have been well reviewed in recent articles [77–84].

Due to the unique electrochemical properties, good electron mobility, highly tunable photophysical properties with various sizes and surface states, and abundant defects and functional groups on their surfaces, CDs are considered to be a competitive nanoemitter in the field of ECL [85]. The ECL activity of CDs was firstly discovered from water-soluble carbon nanocrystals, which released from a graphite rod into aqueous solution by applying a scanning potential [86]. The ECL mechanism of the CDs was proposed to involve the formation of excited-state CD* *via* electron-transfer annihilation of negatively charged $CDs^{\bullet-}$ and positively charged $CDs^{\bullet+}$. The $CDs^{\bullet+}$ were found more stable than $CDs^{\bullet-}$ from stronger cathodic ECL intensity than the anodic value [87]. This is different from microwave-synthesized CDs, whose anodic ECL intensity is larger than the cathodic value, indicating that $CDs^{\bullet-}$ are more stable than $CDs^{\bullet+}$ [88]. Surface straps of CDs are considered to contribute to the ECL emission of these CDs, which often exhibit significantly red-shifted ECL spectrum relative to PL spectrum [89]. In addition, the coreactant ECL mechanisms were exploited to enhance the ECL activity of CDs through reductive-oxidation ECL [90,91] and oxidative-reduction ECL [92,93]. The heteroatom doping is an important strategy to improve the ECL emission of CDs [94,95]. For example, the ECL emission of CDs was significantly enhanced by nitrogen doping, resulting in a broadened band gap and slower decay dynamics, thereby suppressing nonradiative recombination and promoting radiative recombination [95]. Excitingly, amine-rich nitrogen-doped CDs can also acts as the coreactants for $Ru(bpy)_3^{2+}$ ECL generation, showing their eligibility as powerful alternatives to tripropylamine (TPrA) [96]. By covalently coupling the CDs with $Ru(bpy)_3^{2+}$, the hybrid showed a self-enhancing ECL characteristic due to an intramolecular electron transfer process. Recently, CDs have demonstrated their application potential of CDs in ECL biosensing and bioimaging. In this section, we focus on the recent advances in ECL biosensing, and showcase some typical examples.

In order to improve the ECL efficiency of CPDs for ultrasensitive detection of exosomal proteins, surface-plasmon-enhanced ECL system was developed for the determination of pancreatic cancer exosomes based on localized surface plasmon resonance (LSPR) between AuNPs and CPDs (Figure 5A) [97]. The CPDs are non-conjugated polymer dots and synthesized by non-conjugated polyetherimide (PEI) with low carbonization degree, and their luminescent centers are attributed to the formed carbon-core or the molecule/group chromophores [98]. When CPDs@MOF-Ab2 was immobilized on the AuNPs/GCE [97], the ECL intensity was ~4,019 a.u., which obviously increased (Figure 5B, curve f) by a factor of 16 to the case of in the absence of AuNPs (Figure 5B, curve e), demonstrating that LSPR produced by AuNPs greatly enhanced the ECL emission of CPD*. The ECL-LSPR hot electron injection

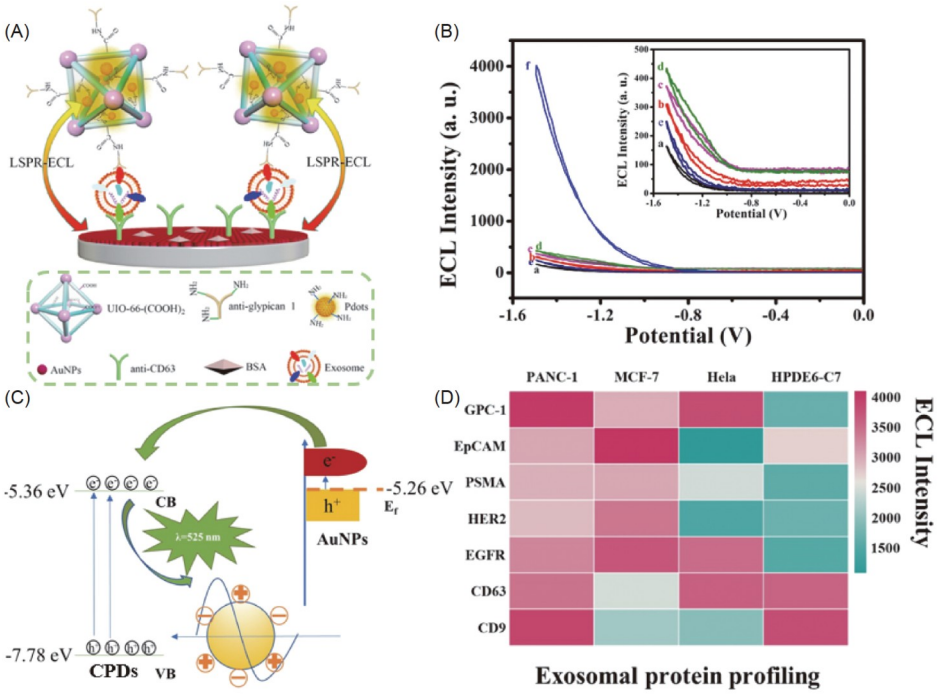

Figure 5 LSPR enhancement of ECL of carbon dots for exosomes detection [97]. (A) Schematic diagram of ECL immunosensor *via* sandwich mode. (B) LSPR enhanced effect evaluation. ECL intensity-potential behaviors of bare GCE (a), AuNPs/GCE (b), CPDs/GCE (c), CPDs@MOF/GCE (d), CPDs@MOF-Ab2/exosome/BSA/Ab1/GCE (e), and CPDs@MOF-Ab2/exosome/BSA/Ab1/AuNPs/GCE (f). (C) ECL-LSPR hot electron injection mechanism. (D) Protein profiling on exosomes derived from PANC-1, MCF-7, HeLa, and HPDE6-C7 cells (color online).

mechanism was proposed to explain this enhancement (Figure 5C). The ECL emission of the CPDs induced AuNPs to generate strong surface plasmon states. Then the excited hot electrons were transferred from the fermi level (E_f) of AuNPs to the conduction band of CPDs, which significantly enhanced the ECL efficiency of CPDs. For loading more amino group-abundant CPDs to one particles, carboxyl group-modified metal organic framework (MOF) was utilized as a carrier. The sandwich-type ECL immunosensor exhibited a high sensitivity with a LOD of 400 particles mL^{-1} and a wide linear range of four orders of magnitude. The LSPR-based ECL immunosensor enabled sensitive multiplex exosomal protein profiling and revealed high selectivity toward different expressions of exosomal surface proteins (GPC-1, EpCAM, PSMA, HER2, EGFR, CD9, and CD63) from several cell lines (PANC-01, HeLa, MCF-7, and HPDE6-C7). A higher expression level of GPC-1 was noticed on tumorous exosomes (PANC-01, HeLa, and MCF-7) than that on non-tumorous exosome (HPDE6-C7) (Figure 5D). The proposed ECL system exhibits a promising platform for exosome protein profiling and early cancer-related diagnosis. Chen *et al*. [99] synthesized nitrogen-doped hydrazide-conjugated CDs and applied them to construct a biosensor for rapid cancer cell detection. The nitrogen atoms were doped into the graphitic cores of CDs for lowering the anodic ECL excitation potential of the CDs due to the upshift of the highest occupied molecular orbital (HOMO) energy level. The ECL efficiency of nitrogen-doped CDs was 2.5-fold higher than that of undoped CDs because the lower potential could notably reduce the side reactions in the ECL process. Using the nitrogen-doped CDs as ECL probe, an ECL biosensor was constructed to detect the cell-secreted hydrogen peroxide through immobilizing the nitrogen-doped CDs on electrode with the help of chitosan, and using Au NPs to bind concanavalin A (Con A) for capturing the cells by binding with the glycosyl on the surface of the cells. Since normal somatic cells and cancer cells secrete and express different levels of hydrogen peroxide, which significantly affects the ECL intensity of the CDs, the ECL biosensor could distinguish cancer cells from normal cells. This work showed that nitrogen-doped CDs was a promising ECL nanoemitter for bioanalysis. Cai *et al*. [100] proposed the synergistic enhancement of cathodic and anodic ECL of GQDs through the coupling between chemical and electrochemical reactions of $K_2S_2O_8$ and Na_2SO_3 as two different coreactants, and constructed an ECL immunosensor for human IgG detection. In this GQDs-Na_2SO_3-$K_2S_2O_8$ system, the enhancement of cathodic ECL was attributed to the chemical reaction between Na_2SO_3 and $K_2S_2O_8$ for generation of additional oxidizing $SO_4^{\bullet-}$ radicals, which reacted with $GQDs^{\bullet-}$ radicals *via* electron-transfer annihilation for generating an excited state (GQDs*). The enhancement of anodic ECL mechanism was proposed that the amount of $SO_3^{\bullet-}$ radicals generated was much more than that produced from electrochemical

pathway, which led to the enhancement of the anodic ECL emission of GQDs. The synchronous ECL enhancement in dual electrodes would be promising for the construction of ECL biosensor. Carbohydrate antigen 15-3 (CA15-3) is one of the most important biomarkers of breast cancer, and it is very important to accurately and sensitively detect low levels of CA15-3. Through fixing the CQDs on polyethyleneimine-functionalized graphene oxide (PEI-GO) to facilitate electron transfer rate and enhance ECL emission, a sensitive sandwich ECL immunosensor was established for the detection of CA15-3 in human serum [101]. The constructed immunosensor showed a linear concentration range from 0.005 to 500 U/mL, with a LOD of 0.0017 U/mL for CA15-3 (signal-to-noise ratio of 3).

5 ECL of Pdots for biosensing and bioimaging

Semiconducting Pdots are defined as a subset of conjugated polymer nanoparticles (CPNs) with size comparable to semiconductor QDs [102]. Pdots need to meet three conditions: (1) their sizes are less than 20–30 nm in diameter, preferably in the 5–20 nm range; (2) they are mainly composed of semiconducting polymers with a volume fraction or weight concentration higher than 50%; (3) they possess a hydrophobic polymer interior [103]. The current methods used to synthesize CPNs include nanoprecipitation, miniemulsions, crystallization-driven self-assembly of amphiphilic block copolymers (CDSA), living CDSA, and microfluidic approach [104]. Nanoprecipitation is the most widely used technique to prepare Pdots with small particle size (<20 nm) and high single-particle brightness. Compared with semiconducting inorganic QDs, Pdots have the potential advantages of nontoxic features and easy functionalization with versatile synthetic strategies. Thus, the electrochemical and ECL behaviors of Pdots have attracted intense scientific attention. As early as 2008, utilizing single molecule spectroelectrochemistry (SMS-EC) technology, Barbara and coworkers [105] studied the ECL of single nanoparticles of conjugated polymer (poly(9,9-dioctylfluorene-co-benzothiadiazole), F8BT) on indium tin oxide (ITO) electrode in acetonitrile solution containing TPrA as coreactant. Compared with conventional ECL on bulk conjugated polymer films, single NP was required to possess longer "build-up" time (~35 s) for the maximum formation rate of ECL. Subsequently, they studied the ECL of oligothiophene nanoparticles in benzene/acetonitrile solution, and revealed the important roles of substituents in regulating the formation of aggregates [106]. However, the analysis application of this system is restricted due to the ECL systems worked in the presence of organic solvent, where the most analytes are present in the aqueous solution. By capping hydrophobic poly[2-methoxy-5-(2-ethylhexyloxy)-1,4-phenylenevinylene] (MEH-PPV) conjugated polymer with the nonionic surfactant Triton X-100, the hydrophilic Pdots (~50 nm) were synthesized by nanoprecipitation, and the ECL behaviors were studied for the first time in aqueous medium [107]. They exhibited annihilation ECL activity upon switching potential between anodic and cathodic potentials. The cathodic ECL of MEH-PPV Pdots was stronger than that of the anodic ECL, which indicated that MEH-PPV Pdot cationic radical ($Pdots^{\bullet+}$) is more stable than Pdot anionic radical ($Pdots^{\bullet-}$), so that MEH-PPV $Pdots^{\bullet+}$ remained active to collide with $Pdots^{\bullet-}$ during cathodic potential scan. The strong anodic and cathodic coreactant ECL emission of Pdots was obtained in the presence of TPrA and $S_2O_8^{2-}$, respectively. The effect of surfactant on the ECL activity of Pdots was further explored. Compared with bare hydrophobic Pdots, nonionic surfactant Triton X-100-capped Pdots enhanced the solubility of Pdots in water, which facilitated the charge (electron or hole) inject from electrodes to Pdots. The ECL activity of the MEH-PPV Pdots capped with other surfactant was also explored, and the results showed that Pdots capped by poly(styrene-co-maleic anhydride) (PSMA) or Pluronic F-127 exhibit much weaker ECL emission than Triton X-100-capped Pdots. Subsequently, this research group synthesized the hydrophilic poly[(9,9-di-(2-ethylhexyl)-9H-fluorene-2,7-vinylene)-co-(1-methoxy-4-(2-ethylhe-xyloxy)-2,5-phenylenevinylene)] (PFV) Pdots capped with Triton X-100, which were similar to the MEH-PPV Pdots described above and exhibited versatile ECL emission in aqueous solution, including annihilation, anodic and cathodic ECL emissions [108]. Ju group [35] synthesized a silole-containing polymer (SCP) by copolymerzation of silole and carbazole *via* Sonogashira reaction and further prepared SCP dots, which showed a band-gap ECL emission at relatively low potential in aqueous solution. Using TPrA as coreactant, the strong anodic ECL emission could be obtained at +0.4 V (*vs*. Ag/AgCl) with a peak value at +0.78 V. This ECL peak potential was far lower than those of the previously reported MEH-PPV dot/TPrA system (+1.10 V) and PFO dot/$C_2O_4^{2-}$ system (+1.90 V), and also lower than commercial $Ru(bpy)_3^{2+}$/TPrA (+1.10 V), surface passivated CdTe QDs/SO_3^{2-} (+0.90 V), and dual-stabilizer-capped CdTe QDs/2-(dibutylamino) ethanol (+0.85 V). The ECL emission could be efficiently quenched through resonance energy transfer from the excited SCP dots to the electro-oxidation product of dopamine. Thus, a low-potential anodic ECL sensing strategy was proposed for ECL detection of dopamine with acceptable performance.

5.1 ECL of Pdots for biosensing

The quenching phenomenon of ECL plays an important role in designing new methodologies for detection of quencher and quencher-related analytes. Based on this effect, different

types of Pdots-modified electrodes have been used in the detection of many small biomolecules, such as dopamine, melamine, H_2O_2, and choline [35,109–111]. Ju and co-workers [35] used ECL of Pdots to detect dopamine based on the resonance energy transfer quenching from the excited SCP dots to the electro-oxidation product of dopamine, which followed the Stern-Volmer equation and produced a sensitive and low-potential ECL sensing method. The quenching constant K_{sv} was found to be 2.3×10^5 M^{-1}. The large value of K_{sv} provided a sensitive ECL detection of dopamine with linear range from 0.050 to 10 μM with an LOD of 50 nM at a signal-to-noise ratio of 3. Very recently, Pdots-based fluorescence (TADF)-ECL was developed for dopamine biosensing, which displayed satisfactory linearity, high selectivity, and high repeatability [109]. The poly(9,9-dioctyfluorenyl-2,7-diyl) (PFO) Pdots possessed strong anodic ECL with $Na_2C_2O_4$ as a coreactant [110]. Based on the fact that the melamine could efficiently quench the ECL signal of the PFO Pdots-$C_2O_4^{2-}$ system, the PFO Pdots-modified electrode was successfully used to determine melamine in commercial milk samples with a wide linear range from 9.0×10^{-11} to 1.1×10^{-8} M and LOD of 2.7×10^{-11} M (signal-to-noise ratio of 3). The quenching mechanism was presumed to be an energy transfer process from the oxidation product of melamine to excited state of PFO Pdots. In addition, the author also found that ECL signal of PFO Pdots could be effectively enhanced by H_2O_2, an important product of various enzymatic reactions. Combining the abundant amine groups of polyamidoamine (PAMAM) dendrimers and the charge transport of fullerene (C60), the ECL biosensor based on C60-PAMAM-PFO nanocomposite was constructed for the detection of H_2O_2 and choline using choline oxidase as the model enzyme [111]. Recently, based on the electrochemiluminescence resonance energy transfer (ERET) strategy, the ECL emission of Pdots at low-trigger-potential was realized by coupling the Pdots with a luminol analogue, *N*-(4-aminobutyl)-*N*-ethylisoluminol (ABEI), and the ABEI-Pdots showed an anodic ECL emission with a low onset potential of +0.34 V and a peak potential at +0.45 V (*vs*. Ag/AgCl). This low-triggering-potential ECL for imaging detection of glucose in buffer and serum showed an LOD of 3.3 μM and excellent selectivity [112].

Capsulizing a large amount of ECL molecules into one nanoparticle for single-target recognition can greatly improve the sensitivity of the ECL assay. The $Ru(bpy)_3^{2+}$-incorporated Pdots (RuPdots) were firstly designed by utilizing luminescent conjugated polymer as a carrier to encapsulate a large amount of hydrophobic $Ru(bpy)_3[B(C_6F_5)_4]_2$ as ECL molecules into individual Pdot for coupling high loading amplification and ERET-enhanced ECL (Figure 6a) [113]. The RuPdots with an average size of 20 nm and encapsulation of about 1,350 $Ru(bpy)_3^{2+}$ molecules into individual Pdot showed greatly enhanced ECL emission. Using TPrA as a coreactant, the ERET from the excited polymer dots to the encapsulated $Ru(bpy)_3^{2+}$ was demonstrated, leading to a 15.7-fold higher ECL emission (Figure 6c, green curve) than that of $Ru(bpy)_3^{2+}$ with the same amount at the gold electrode (Figure 6c, blue curve). By coupling DNA-functionalized RuPdots as a nanoprobe for signal acquisition and a ligase reaction to endow specificity of the detection, the proposed ECL method for detection of single nucleotide polymorphisms (SNP) showed high sensitivity and excellent specificity (Figure 6b). Using mutant *KRAS* gene as a model target, the ECL biosensor showed a linear range from 1 fM to 1 nM with an LOD of 0.8 fM (signal-to-noise ratio of 3). Moreover, the ECL intensity could be used to clearly distinguish mutant *KRAS* gene and wild-type *KRAS* gene at different concentrations. Even at a concentration of 1 fM, the ECL intensity for mutant *KRAS* gene was 2.5 times that for wild-type *KRAS* gene (Figure 6d). This work showed that dye-doped Pdots could be used as a universal label for ultrasensitive ECL SNP detection [113]. Recently, an ECL biosensor based on carboxyl-functionalized Pdots was proposed for ultrasensitive detection of miRNA-122 by coupling two-step signal amplification strategy including duplex-specific nuclease (DSN) enzyme-assisted amplification and rolling circle amplification (RCA) [114]. It should be pointed out that this carboxyl-functionalized Pdots were not prepared by nanoprecipitation with exogenous functionalized reagents, but reasonable linking of polymer and carboxyl group on the side chain. This ECL biosensor had a wide linear range of 0.1 fM to 100 pM, and the LOD was calculated to be 36 aM (signal-to-noise ratio of 3).

Generally, ECL bioassays are conducted in the presence of a coreactant, which may cause an inevitable error and a lack of reproducibility in detection, especially when using dissolved oxygen as an endogenous coreactant. The coreactant-free ECL of carboxyl-functionalized Pdots were used for ultrasensitive detection of microRNA by integrating target-catalyzed hairpin assembly and enzyme-triggered DNA walker recycling amplification. Based on the efficient quenching ability of BHQ on quantum dots, the ECL biosensor exhibited high sensitivity, high selectivity and stability for miRNA detection [115].

5.2 ECL of Pdots for bioimaging

Due to highly efficient ECL emission from Pdots with coreactant, the ECL imaging method can be used to detect various types of analytes, such as metal ions, proteins, nucleic acid, and living cells. The cyanovinylene-contained Pdots were first employed for ECL imaging analysis of metal ions [116]. Due to an electron-withdrawing cyano group on polymer backbone of *p*-phenylenevinylene for enhancing the luminescent efficiency, the poly[2-methoxy-5-(2-ethylhexyloxy)-1,4-(1-cyanovinylene-1,4-phenylene)] (CN-PPV)

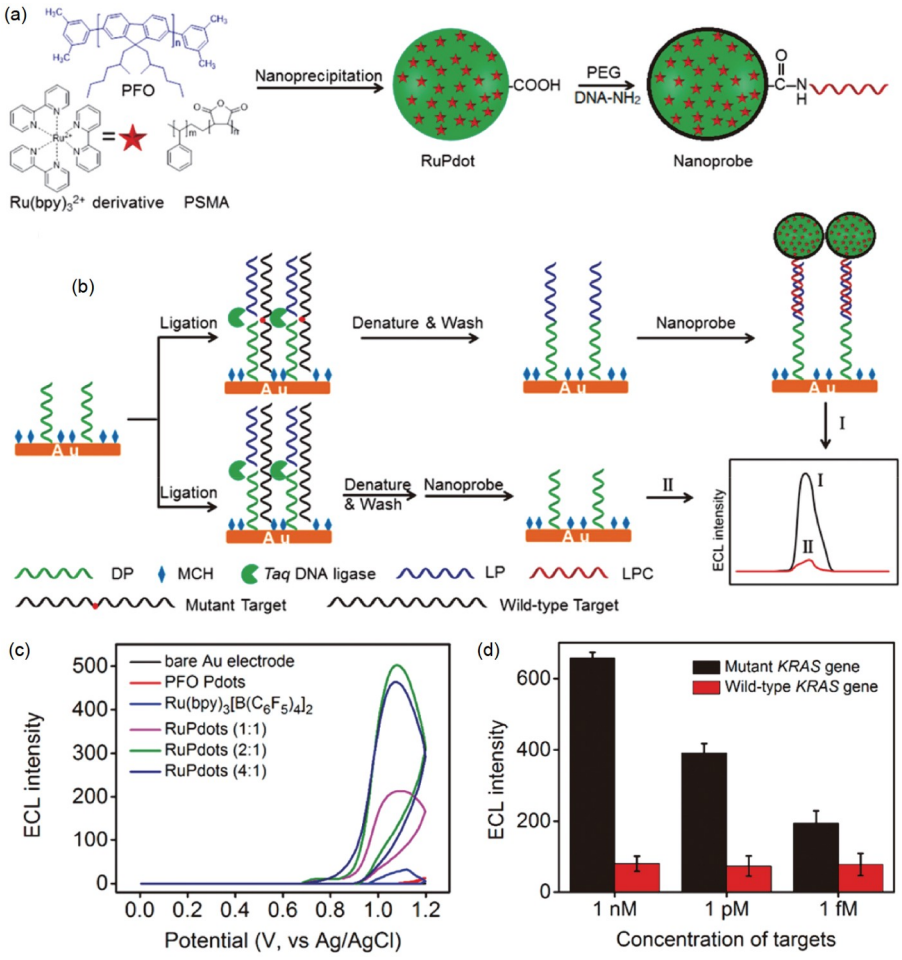

Figure 6 ERET-enhanced ECL generation from Pdots for detection of single-nucleotide polymorphism [113]. Schematic diagrams of preparation of RuPdot nanoprobe using PFO, hydrophobic $Ru(bpy)_3^{2+}$ derivative, and PSMA (a); SNP detection with ligase detection reaction and nanoprobe (b). (c) ECL curves of bare and modified Au electrodes. (d) ECL intensity for mutant *KRAS* gene and wily type *KRAS* gene at 1 nM, 1 pM, and 1 fM. ECL measurements of the modified Au electrodes were conducted in 0.10 M pH 7.0 PB containing 100 mM KNO_3 and 30 mM TPrA at 100 mV/s (color online).

Pdots exhibited high ECL efficiency in aqueous solution with tri-*n*-propylamine as coreactant. Based on different chelating interactions of metal ions and the Pdots, the proposed ECL imaging method showed excellent analytical performance for Fe^{3+} with a wide linear range from 100 pM to 100 μM with an LOD of 67 pM. Compared with the traditional intensity-based analysis, this imaging-based method featured the advantages of simplicity, rapidity, and high-throughput, and thus extends the ECL application of Pdots.

Due to the high luminescence efficiency of Pdots, a true-color ECL imaging strategy was developed for multi-immunoassay of proteins by dual DNA amplification [117]. The self-quenched probe was designed by functionalizing the Pdots with DNA1 and then hybridizing with black hole quencher (BHQ)-labeled DNA2 to DNA1. The BHQ provided high quenching efficiency of the Pdots for "off-on" imaging with low background and the evaporation of gold film (5 nm chrome followed by 50 nm gold) on ITO electrode greatly enhanced the ECL emission of Pdots for about 100 folds. By sandwich immunorecognition, a biotinylated secondary antibody was immobilized on the electrode surface for capturing streptavidin and subsequent biotin-labeled primers. Through coupling rolling circle amplification (RCA) and enzymatically cyclic release (ECR), a dual DNA-amplified ECL signal was achieved by releasing the Pdots from the self-quenching probe into detection solution. Using carcinoembryonic antigen, cytokeratin-19-fragment, and neuron-specific enolase as a lung cancer-specific biomarker panel, the ECL imaging-based multi-immunoassay showed wide linear range of 1 pg/mL to 500 ng/mL with LODs of 0.17, 0.12, and 0.22 pg/mL, respectively. The proposed method could accurately detect these biomarkers in clinical human serum samples for lung cancer screening.

Because the occurrence and development of a disease are usually accompanied by the abnormality of multiple markers, simultaneous detection of multiple nucleic acids possesses potential importance in the classification and diagnosis of diseases [118,119]. A potential- and color-

resolved ECL system from two Pdots was developed for array imaging of multiplex microRNA [120]. The luminol-doped polymer dots (L-Pdots) were used as the low-potential emitter at +0.6 V for blue light ECL (425 nm), while the diethylamine-coupled Pdots (N-Pdots) were used as a high-potential emitter at +1.0 V for red light ECL (675 nm). Compared with traditional potential-resolved ECL system, the interference of threshold produced by the low potential emitter at high potentials could be avoided by splitting the true-color photograph of ECL imaging for Pdots into red, green, and blue (RGB) channel. This dual-resolved strategy could improve the accuracy of simultaneous detection of two markers without interfering with each other. By covalently binding quencher-labeled DNAs specific to miRNA-21 and miRNA-205 with two Pdots, simultaneous detection of two microRNA was achieved through target-initiated cycle for "off-on" signal amplification with duplex-specific nuclease. By extracting the intensity values of ECL images in the blue and red channels, miRNA-21 and miRNA-205 could be quantified respectively, showing high sensitivity, good selectivity, excellent accuracy and acceptable precision towards cell lysates and spiked miRNAs in human serum samples. The results demonstrated great potential of the proposed potential- and color-resolved ECL strategy for simultaneous detection of multiple markers.

In order to further improve the ECL efficiency of Pdots, a dual intramolecular resonance energy transfer (RET) in triple-component polymer dots was designed to enhance ECL for simultaneous visual analysis of two kinds of membrane proteins on living cells [121]. The triple-component Pdots were composed of carbazole, tetraphenylethene (TPE), and 2,2-difluoro-3-(4-methoxyphenyl)-4,6-diphenyl-2H-1,3l4,2l4-oxazaborinine (DMDO). The first intramolecular RET occurred between carbazole moiety as donor (D1) and TPE that acted as both acceptor (A1) and donor (D2). Then the energy was transferred from TPE moiety to DMDO (A2) through a second intramolecular RET process. Compared with no and single RET, dual RET mechanism could greatly promote the ECL for about 380 and 31 times, respectively. By integrating the probe with target-mediated enzymatic circulation amplification and DNA arrays, the triplet-component Pdots were carried on metal-organic frameworks (MOF) as sensitive ECL probe for simultaneous visual analysis of two kinds of proteins, mucin 1 and human epidermal growth factor receptor 2, which exhibited a sensitive and specific quantification of membrane proteins with LOD in pg/mL level.

However, the ECL imaging technology is difficult to be applied in cytosensing and microscopic imaging due to the demand for transporting coreactant with high concentration to emitter and the limitation of short lifetime of the radicals [122,123]. Therefore, the development of ECL systems with high ECL efficiency, low cytotoxicity, and no additional coreactant has naturally become an urgent need in this field. Ju and co-workers [124] designed a dual intramolecular electron transfer strategy and tertiary amine conjugated polymer dots (TEA-Pdots) to develop a coreactant-embedded ECL system of Pdots for microimaging of membrane protein on living cells (Figure 7). The coreactant-embedded TEA-Pdots were synthesized by coupling the diethylamine as anodic coreactants with bone of poly[(9,9-dioctylfuorenyl-2,7-diyl)-alt-co-(1,4-benzo-{2,1′,3}-thiadiazole)] (PFBT) followed by nanoprecipitation with poly(styrene-co-maleic anhydride) (PSMA) (Figure 7a). After direct covalent coupling of two coreactants TEA molecules to the light-emitting unit, the coreactant-embedded Pdots showed unprecedented ECL intensity, which was 132 and 45 times stronger than those from the mixture of Pdots with TEA at equivalent and 62.5 times higher amounts (Figure 7b), respectively, and even 4-fold higher than that of typical $[Ru(bpy)_3]^{2+}$ system. This remarkably enhanced ECL emission of Pdots is due to the shortened electron transfer pathway and reduced complication of radical intermediates transport in intermolecular electron transfer-based ECL process. The dual intramolecular electron transfer mechanism was proposed to explain this enhancement, that is, the first intramolecular electron transfer from $TEA^{\bullet}$ to PFBT and the second intramolecular electron transfer from $PFBT^{\bullet-}$ to another $TEA^{\bullet+}$ (Figure 7c). By using membrane protein human epidermal growth factor receptor 2 (HER2) as a target, this coreactant-embedded system successfully achieved *in situ* ECL microimaging of protein on single living cells. Compared with labelled cells, this coreactant-embedded SA@TEA-Pdots system showed the bright image of whole cell membrane (Figure 7d), while the ECL signal only around cell periphery for SA@PFBT Pdots system (Figure 7e). The latter was due to the hindered diffusion of coreactant through the plasma membrane. The proposed coreactant-embedded ECL system has obvious advantage in membrane protein imaging on living cells without extra coreactant, permeable treatment, and modification of the electrode. Combining the advantages of microfluidic technology with ECL imaging, this coreactant-embedded Pdots was further used for imaging of single cell secretions on the confined ECL imaging microarray (CEIM) chip [125]. The CEIM chip was designed to capture single or a few cells in each cylindrical microwell for quantitation of cell-secreted dopamine. The coreactant-embedded Pdots were functionalized with dopamine aptamer for *in situ* recognizing of cell-released dopamine. Based on the efficient quenching of ECL emission from the Pdots by electrochemical oxidation product of the captured dopamine, the detection of dopamine secreted from single PC 12 cell was conducted under hypoxia stimulation. These studies provided new avenue for ECL enhancement and a powerful tool for single living cell analysis and dynamic study of biological events.

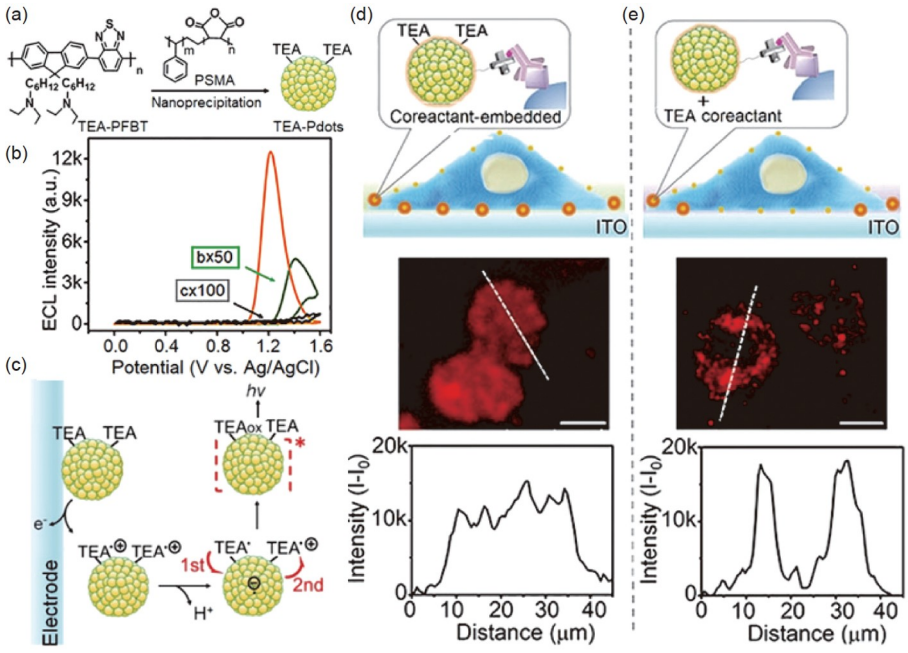

Figure 7 Intramolecular electron transfer strategy for amplifying ECL of Pdots for *in situ* ECL microimaging of membrane protein on single living cells [124]. (a) Preparation of TEA-Pdots. (b) ECL comparison: 50 μg/mL TEA-Pdots (orange), 50 μg/mL PFBT Pdots+160 μM TEA after magnified for 50 times (green), and 50 μg/mL PFBT Pdots after magnified for 100 times (black). (c) Intramolecular electron transfer mechanism of TEA-Pdots. ECL microimaging of human epidermal growth factor receptor 2 (HER2) on living SK-BR-3 cells treated with SA@TEA-Pdots (d) and SA@PFBT Pdots (e) in presence of 0.1 M TEA (color online).

Currently, Pdots as a new type of ECL nanoemitters are still in a period of rapid development. The future development of Pdots includes: (1) exploiting more highly ECL efficient and stable Pdots, especially featured with low potential, wavelength resolution, multiplex colors; (2) designing intelligent, integrated, flexible and portable ECL chip device through combining with other techniques, such as microfluidics; and (3) exploring robust application, especially involving biological processes.

6 ECL of aggregation-induced emission nanoparticles (AIE dots) for biosensing

Aggregation-induced electrochemiluminescence (AIECL) is a new concept that combines the properties of aggregation-induced emission (AIE) of luminophores and ECL technology to guide the design of efficient ECL luminescent materials. AIE refers to the phenomenon that the luminophores often show no emission at the molecular state but become brightly emissive at aggregated state [126–128]. In 2017, De Cola's group [129] defined AIECL and reported that the ECL emission of aggregated planar platinum (II) complexes was greatly improved compared with that before aggregation. As a strategy to improve the ECL efficiency, AIECL has achieved rapid progress in the development of ECL luminophores, biosensing, ECL mechanism research, cell imaging, and environmental monitoring [36]. In recent five years, many AIECL luminophores have been reported based on their excellent luminescent behaviors at the aggregated state. AIE dots are usually biocompatible nanoparticles with a dense core of AIE fluorogens (AIEgens) and protective shells, in which AIEgens greatly determine the performance and function of the AIE dots [37,130,131]. Herein, we mainly introduce the AIE dots that refer to small size organic nanoparticles including small organic molecule dots and polymer dots.

The ECL emission of small organic molecules appears mostly due to the structure of polycyclic aromatic hydrocarbons (PAHs), except for luminol. PAHs also play an important role in the development of ECL nanoemitters because of their modifiable structure, easy adjustment of emission wavelength and nontoxicity. However, due to the large planar conjugate structure and the strong π-π accumulation of molecules in aggregated state, their emissions present the aggregation-caused quenching (ACQ) effect, which seriously hinders their development in ECL analysis.

In 2017, Qi group [132] synthesized organic nanoparticles of coumarin derivative 6-[4-(*N*,*N*-diphenylamino)phenyl]-3-ethoxycarbonyl coumarin (DPA-CM) based on donor-acceptor structure, with an average particle size of 5.82 nm. Compared with DPA-CM in organic solution, DPA-CM NPs showed a red shift of absorption wavelength and a blue shift of PL wavelength, as well as the AIECL in aqueous solution. The enhancement of ECL emission was caused by the small size of DPA-CM NPs, the restrictive conformational

relaxation of NPs and the good stability of cationic radical. Using TPrA as a coreactant, DPA-CM NPs-modified electrode showed a good linearity for the detection of ascorbic acid (AA), uric acid (UA) and dopamine (DA) in the concentration range of 0.05–50 μM, with LODs of 0.04, 0.2 and 0.4 μM, respectively. Subsequently, the research of AIECL based on small organic molecules has developed rapidly, and the design and development of AIECL luminophores mainly focus on the AIEgens, such as tetraphenylethylene (TPE), hexaphenylthiazole and carborane. In 2019, Zhuo and co-workers [133] synthesized hexagonal tetraphenylethylene microcrystals (TPE MCs) and studied their ECL properties for the first time. Compared with TPE molecule, the ECL of TPE MCs was significantly enhanced. Combined with the mechanism of AIE, they proposed the mechanism of intramolecular motion restriction (RIM) to enhance ECL. They combined TPE MCs with target-activated bipedal DNA walker to construct a highly sensitive ECL biosensor for Mucin 1 assay, which was the first example of TPE applied to ECL biosensing. They also observed the near-infrared ECL emission based on TPE nanocrystals (NCs), which showed better ECL efficiency and biocompatibility [134].

Recently, Lu and co co-workers [135] synthesized a series of tetraphenylbenzosilole (TPBS) derivatives with different substituent groups (TPBS-H, TPBS-B, TPBS-M, TPBS-F, TPBS-C), and systematically investigated the influence of substituents on their AIECL behaviors. Among them, TPBS with electron-withdrawing cyano groups (TPBS-C) showed the most excellent ECL emission. Based on the principle that electrons in the reduction process of TPBS-C can be captured by Cr (VI) to inhibit ECL emission, the sensing method of toxic Cr (VI) was designed and realized with a wide linear range from 10^{-12} to 10^{-4} M and an extremely low LOD. Li group [136] reported a quaternary ammonium salt groups-functionalized AIEgen (QAU-1). The coating QAU-1 showed significant cathodic ECL emission compared with the dissolved state. They further constructed a bleomycin-responsive ECL biosensor (Fc-DNA/QAU-1/ITO) through combining it with target-initiated specific cleavage. The QAU-1 was labeled with Fc-DNA, which contained a sequence recognized by bleomycin, and the ECL emission was quenched by Fc due to the resonance energy transfer and electron transport effects. With the addition of bleomycin, Fc-DNA was selectively cleaved and released from QAU-1 to regain the ECL.

Recently, Qi group [137] reported the AIECL of tetra[4-(4-cyanophenyl) phenyl] ethene (TCPPE) and developed its application in three biothiol assays (Figure 8A). TCPPE exhibited a clear AIECL behavior when it transferred from good solvent (CH_3CN) to poor solvent (water), while the later gradually formed the uniform aggregate with the increase of f_w (Figure 8B). Moreover, the normalized ECL spectra of TCPPE NPs-$S_2O_8^{2-}$ in different f_w values showed that the maximum ECL wavelength red-shifted from 505 to 526 nm with the increase of f_w from 40% to 90% (Figure 8C). The authors also observed the phenomenon of aggregation-induced ECL chromic emission (AI-ECLC) for TCPPE NPs, where the color of ECL emission changed from cyan to yellow-green with the increasement of f_w. Due to the reactivity of the sulfhydryl groups or carboxyl groups within biothiols, $SO4^{\bullet-}$ inhibited the ECL emission of TCPPE NP, and thus an ECL method was proposed for the determination of three biothiols with LODs of 6, 7, and 300 nM for cysteine (Figure 8D), homocysteine, and glutathione, respectively.

Compared with the small molecules, conjugated polymers have advantage of amplifying the luminescence properties of monomers, easy synthesis and convenient adjustment of luminescence properties through structural modification of monomers [138,139]. As mentioned in the previous section, the most widely used Pdots are greatly reduced the luminescence efficiency in the aggregation process. The introduction of AIE active unit is a good choice to develop Pdots with high ECL efficiency. At present, AIE active polymers used in ECL mainly include the following categories according to their molecular composition: fluorenyl, carbazole, benzothiadiazole (BT) and boron hetero β-diketone derivative polymer and TPE conjugated polymer.

In 2018, Ju and co-workers [140] reported the sensing application of AIECL from three-component Pdots containing AIE-active moiety. This donor-acceptor polymer was synthesized with TPE derivative, 9-(diphenylmethylene)-9H-fluorene (DPF), as AIE active unit and energy resonance transfer (RET) receptor, fluorene unit as RET donor and binaphthol structure as linker. The intramolecular fluorescence resonance energy was transferred from fluorene to DPF, and showed obvious yellow fluorescence emission at 543 nm. Moreover, with the increase of water content, both ECL and fluorescence showed the enhanced emission. The prepared Pdots showed stable anodic ECL emission with TEA as coreactant, and the ECL could be quenched by Rhodamine B through energy resonance transfer. Thus they constructed an "off-on" ECL aptasensing strategy to realize the highly sensitive detection of Pb^{2+} with an LOD of 38.0 pM [140]. This work laid the groundwork for the future application of Pdots in AIECL biosensing. Xu and co-workers [141] subsequently reported the AIECL behavior of another AIE active Pdots of polyfluorene derivative containing TPE in aqueous solution. Compared with polyfluorene nanoparticles, the introduction of TPE unit limited the free rotation of benzene rings in molecules and hinders the π-π stacking interaction between molecules, which significantly improved the ECL emission. Subsequently, a three-component polymer was designed and synthesized differently by respectively adjusting fluorene units and carbazole units as electron donors, in which carbazole could act as an electron donor [142]. The ECL test showed that car-

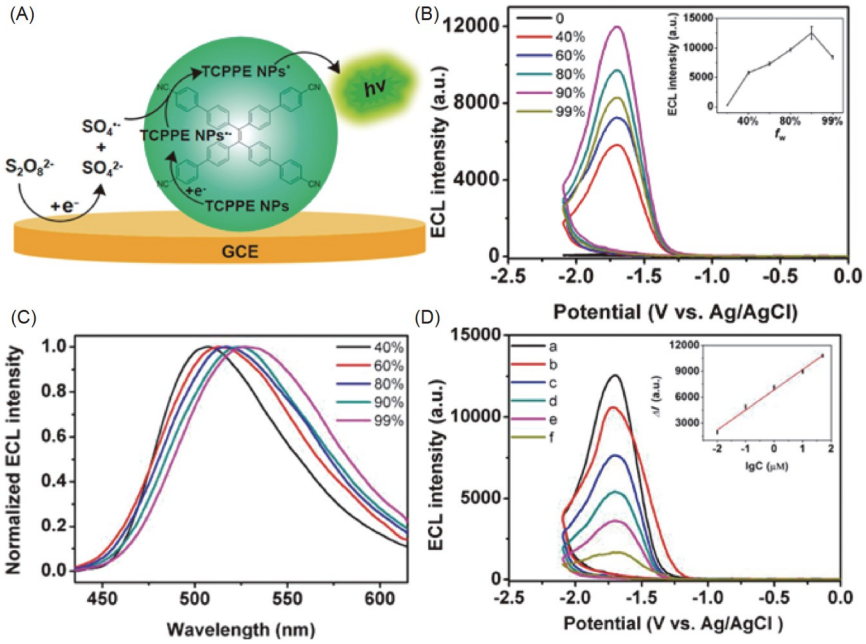

Figure 8 Aggregation-induced enhanced ECL of cyanophenyl-functionalized tetraphenylethene nanoparticles for biothiol analysis [137]. (A) Proposed ECL mechanism of TCPPE NP with $K_2S_2O_8$ as a coreactant. (B) ECL intensity *vs*. potential profile of 2 μM TCPPE in CH_3CN/Bz (*v*/*v*=1:1) containing 45 mM BPO (f_w=0) and ECL intensity *vs*. potential profiles of 2 μM TCPPE NPs at different f_w (f_w=40%, 60%, 80%, 90%, and 99%) in 0.1 M PBS (pH 7.4) containing 45 mM $K_2S_2O_8$. Scan rate: 0.1 V/s, PMT=−600 V (inset: ECL intensity of TCPPE NPs with different f_w). (C) Aggregation-induced ECL chromic emission. Normalized ECL spectra of TCPPE NPs with different f_w in 0.1 M PBS containing 45 mM $K_2S_2O_8$ and 2 μM TCPPE NPs. (D) ECL intensity *vs*. potential profiles of TCPPE NP-modified GCE for different concentrations of cysteine: (a) blank, (b) 0.01 μM, (c) 0.1 μM, (d) 1.0 μM, (e) 10 μM, and (f) 50 μM (inset: calibration plot of cysteine) (color online).

bazole-based Pdots had high AIECL efficiency and low oxidation potential. It increased the HOMO energy level and reduced the lowest unoccupied molecular orbital (LUMO) energy level of polymer, making it easier for holes and electrons to be injected into the conjugate backbone and conducive to the ECL reaction. This study provided a strategy for the development of AIECL Pdots with low potential and high ECL emission intensity *via* adjusting the D-A electronic structure. They further introduced dual intramolecular resonance energy transfer mechanism in carbazole based AIECL Pdots to realized higher ECL emission, which showed 23.1% relative AIECL efficiency (*vs*. 1 mM $Ru(bpy)_3^{2+}$) [121]. By combining with target-mediated enzymatic circulation amplification and DNA arrays, in which metal–organic frameworks were used to carry the Pdots as ECL probes, an ECL imaging method was successfully designed for simultaneous visual analysis of two kinds of proteins on living cell surface, which expanded the application of AIECL Pdots in ECL imaging and biological analysis.

At present, many reported AIECL signals of Pdots are unstable. In order to better apply them to bioanalysis, it is necessary to design AIECL Pdots with efficient and stable signals. Xu and co-workers [143] designed and synthesized the AIE active Pdots with excellent ECL stability for ultrasensitive nucleic acid assay. The AIE-active Pdots consist of two monomers, TPE and BT. The former acted as a typical AIE-active moiety for enhancing the luminescence intensity in the aggregated states, and the latter featured excellent redox reversibility and rigid structure to provide good stability. The Pdots exhibited good ECL stability for the consecutive scans of twenty cycles with a relative standard deviation (RSD) of 0.6%. By combining two recycling amplification strategies, duplex-specific nuclease (DSN)-assisted target recycling amplification and catalytic hairpin assembly (CHA), an ECL biosensor based on the ERET quenching mechanism was constructed for ultrasensitive detection of miRNA-21 with an LOD of 32 aM. This work provided useful reference for designing stable AIE-active Pdots.

Similar to BT, boron hetero β-diketone derivative as an important electron acceptor, has also attracted extensive attention in the field of optoelectronic materials. In 2020, Hua and co-workers [144] designed a new donor-acceptor type of AIECL Pdots for an accurate uranyl ion (UO_2^{2+}) monitoring utilizing a portable ECL system, which took TPE as the donor and hetero β-diketone derivative as receptors. After modified with ssDNA, the Pdots could capture UO_2^{2+}, which effectively amplified the ECL signal of Pdots through resonance energy transfer mechanism. This strategy realized highly sensitive detection of UO_2^{2+} with an LOD of 10.6 pM, indicating application potential in the field of environment monitoring.

7 ECL of other nanoemitters for biosensing and bioimaging

7.1 Luminophore-doped silica nanoparticles

Luminophore-doped silica nanoparticles are a kind of luminescent nanomaterials obtained by coating or embedding organic or inorganic molecules into silica. These molecules interact with the silica body through chemical bond or simple physical coating to form composite materials. So far, many kinds of organic or inorganic luminophores have been successfully doped into silica nanoparticles. Compared with a single molecule, the luminescent intensity of doped silica nanoparticles can be markedly increased. As a protective shell, silica can prevent luminophore molecules from contacting directly with the external environment, hinder the infiltration of oxygen molecules, effectively slows down photobleaching and reduce the degree of fluorescence quenching, thus improving the photostability. Compared with QDs, luminophore-doped silica nanoparticles have high stability, water solubility, low toxicity, high sensitivity and rapid reaction ability, and they are easy to connect functional groups such as amino or carboxyl groups. Up to now, this kind of nanoparticles has been widely used in the fields of chemical analysis, environmental monitoring and biosensing [145]. Luminophore-doped silica nanoparticles have proved to be attractive in ECL analysis, owing to the following advantages: (1) thousands of luminophore molecules can be loaded inside the nanoparticles to improve the luminous efficiency; (2) the synthetic scheme is simple and universal, and has good stability in water; (3) the surface is usually functionalized with amino and carboxyl groups, which is convenient for bioconjugation [20]. The most common luminophores doped in silica nanoparticles are $Ru(bpy)_3^{2+}$ and its derivatives. The preparation methods can be divided into Stöber method and reverse microemulsion method. Thanks to the high ECL efficiency, good stability and biocompatibility, many Ru@SiNPs-based ECL biosensors have been reported [146–151].

Single-molecule techniques can reveal the heterogeneity and stochastic processes of biological systems through providing far richer information. ECL imaging of individual biomolecules remains a challenge because of the weak ECL emission from the luminophore itself. Therefore, there is a need to develop nanoemitter complexes with high ECL efficiency. Recently, Liu *et al*. [152] synthesized $Ru(bpy)_3^{2+}$-doped silicon nanoparticles (RuDSNs) to couple with AuNPs for the preparation of RuDSNs/AuNPs nanoemitter. The presence of a large number of inner active $Ru(bpy)_3^{2+}$ molecules in individual nanoparticle (~3.6×10^4 dyes per NP) increased the ECL intensity, and the decoration of AuNPs further enhanced the ECL signal (~2-fold). Using cytokeratin CK19 as the model target, the ECL imaging of a single biomolecule was realized based on the idea of "one protein to one nanoemitter" through sandwich immunoassay (Figure 9a). The signal-to-noise ratio in the ECL imaging of single biomolecule was ~17-fold higher than that of PL imaging, mainly due to the low background of the ECL technique and the more stable luminescence of RuDSNs/AuNPs compared with dyes. Based on the successful discrimination of a single antigen molecule by ECL imaging, the authors realized the detection of different antigen concentrations by counting the number of ECL spots, which increased as the concentration of CK19 increased and reached a plateau at a concentration of 20 ng/mL (Figure 9b). The linear range was 0.01–10 ng/mL with an LOD of 0.12 pg/mL (Figure 9c). Such a low LOD is attributed to the low background of the ECL and the signal amplification at RuDSNs/AuNPs. Furthermore, the constructed ECL system had high specificity for the detection of CK19 proteins (Figure 9d). This work demonstrated that the design of more efficient ECL nanoemitters was critical for realizing ultrasensitive ECL analysis, especially for single biomolecule detection.

7.2 Metal-organic frameworks (MOFs) and covalent organic frameworks (COFs)

As porous crystalline materials, MOFs have attracted extensive attention in the fields of gas adsorption, heterogeneous catalysis, chemical sensing and nano medicine [153,154]. However, due to the low conductivity, lack of modification sites and poor biocompatibility, its application in the field of ECL sensing is limited. In recent years, many literatures have reported the design strategies of MOFs composites with ECL activity, including post synthesis modification [155], *in-situ* assembly of ECL phosphors in the framework [156], using ECL luminophores as ligands [157], and lanthanide MOF [158,159].

The first type is the post synthesis modification. For example, MOFs-enriched CdTe QDs were used as an efficient ECL probe for the detection of trace biomarkers. The MOFs were used as the carrier of CdTe QDs, and the ligand 2-aminoterephthalic acid acted as a coreactant catalyst for the conversion of $S_2O_8^{2-}$ to $SO_4^{\bullet-}$ and further enhanced the ECL emission of CdTe [160]. Using MOF-enriched CdTe QDs to label antibody, a sandwich immunosensor for cardiac troponin-I antigen was constructed with an LOD of 0.46 fg/mL. The second type is the *in-situ* assembly of ECL luminophores in the framework of MOFs. For example, glutathione (GSH)-modified AuNCs were used as one of the units to construct the GSH-AuNCs-based MOFs by coordination self-assembly, which not only inhibited the non-radiative transition caused by ligand rotation, but also dispersed the spatial distribution of AuNCs and reduced the ACQ effect [161]. Compared with GSH-AuNCs, the anodic ECL efficiency of GSH-AuNCs-based MOFs was 10 times higher. The proposed sensing platform for rutin achieved an LOD of

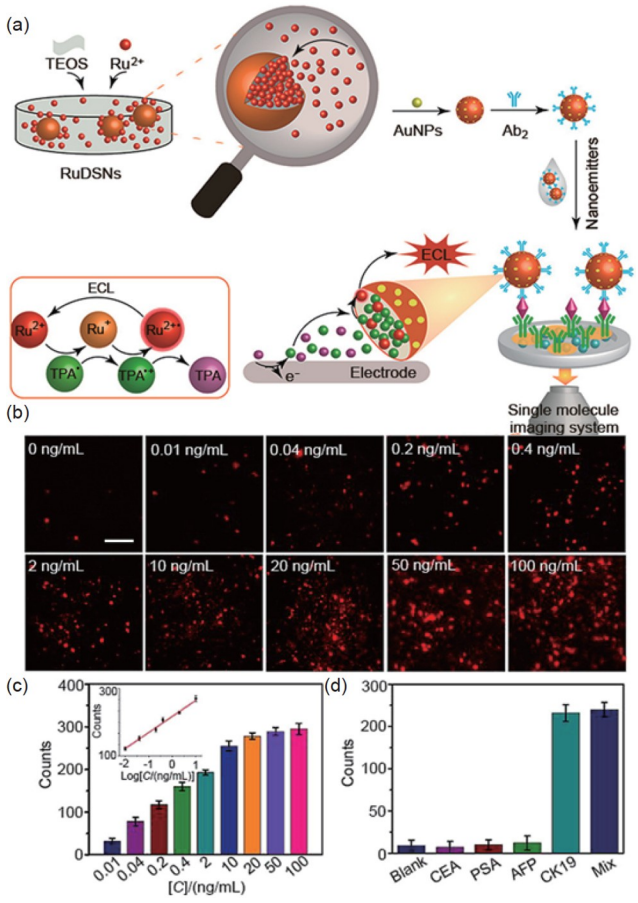

Figure 9 Nanoemitters complexes for single biomolecule detection [152]. (a) Schematic illustration for single-protein-molecule imaging by ECL. (b) Single molecule ECL imaging of various concentrations of CK19 on the ITO electrode surface revealed by the emission from RuDSN/AuNPs. (c) ECL counts calculated with different concentrations of CK19 from 0.01 to 100 ng/mL. Inset: linear relationship between ECL counts and the logarithm of CK19 concentration in the range from 0.01 to 10 ng/mL. (d) Specificity tests with interfering proteins (40 ng/mL) and target CK19 protein (0.4 ng/mL). CEA: carcinoembryonic antigen; PSA: prostate specific antigen; AFP: alpha fetoprotein; Mix: the mixture of 40 ng/mL of interfering proteins (CEA, PSA, and AFP) and 0.4 ng/mL of CK19. Scale bar: 5 μm (color online).

10 nM. The third type is the frameworks composed of ECL luminophore as ligand. With benchmark ruthenium complex as a ligand, the redox-active MOF was first designed for generating stable ECL emission. It exhibited good electron transfer ability between the MOF and coreactant, and was used for the detection of cocaine in the serum sample with good performance [162]. To further improve the ECL emission, Lei and co-workers [163] designed a mixed-ligand MOF (m-MOF) by integrating two ligands, one as a luminophore and the other as a coreactant. Compared with single-ligand MOF, m-MOF exhibited significantly higher ECL emission, which was attributed to the efficient intrareticular electron transfer between the two ligands within the MOF. In addition, lanthanide MOFs were found to be a class of ECL-active nanomaterials, in which ECL behavior could be efficiently tuned by lanthanide metal nodes and peripheral organic ligand. Very recently, the anodic ECL of europium-based MOFs [158] and the cathodic ECL of terbium-based MOFs [159] were explored for ECL immunoassay and showed excellent application prospects.

Covalent organic frameworks (COFs) are a class of crystalline porous organic polymers by linking organic molecules together through strong covalent bonds. Compared with MOF, metal-free COFs avoid the ECL quenching effect of metal nodes and have better water stability owing to the strong covalent bonds. COFs have been recently exploited as new ECL emitters [164,165]. Xiao and co-workers [164] explored the ECL generation from pyrene-based sp^2 carbon COF, which was constructed by C=C polycondensation of tetrakis(4-formylphenyl) pyrene (TFPPy) and 2,2′-(1,4-phenylene) diacetonitrile. The ultrathin nanosheets of this COF showed highly efficient and stable ECL emission in cathodic potential scan with $S_2O_8^{2-}$ as a coreactant and Bu_4NPF_6 as a coreaction accelerator. The authors attributed the COF structure to shortening the transport distance between electrons, ions, and coreactant, as well as introducing AIEgens to reduce the ACQ effect. Based on the efficient quenching of ferrocene on the ECL emission of the COF nanosheet, an ECL biosensor was constructed for the determination of miRNA-21 with a linear response from 100 aM to 1 nM and a low LOD of 46 aM. Recently, Lei and co-workers [165] designed a donor-acceptor COF as ECL emitter by integrating triazine and triphenylamine as donor and acceptor units in the reticular structure, respectively. This D-A COF showed hundred-fold ECL enhancement compared with its benzene-based COF with small D-A contrast, owing to the rapid intrareticular charge transfer (IRCT) within D-A COF. Significantly, dual ECL emission peaks of this COF were obtained through the coreactant-mediated oxidation at relatively low potential and the direct oxidation at high potential. These studies indicated that COF dramatically enhanced ECL emission through efficient intrareticular charge transfer, and can become promising luminophores in the future.

7.3 Metal nanoclusters

Gold and silver nanoclusters (NC_S) have been the research hotspot of ECL in recent years. They are often composed of several to dozens of atoms, and are green luminaries with good biocompatibility, unique catalytic, optical and electrochemical properties [29]. Wang and co-workers [166] reported the near infrared ECL of rod bimetallic $Au_{12}Ag_{13}$ NCs. The ECL intensity of the annihilated state was about 10 times higher than that of $Ru(bpy)_3^{2+}$. Meanwhile, its coreactant ECL emission was about 400 times stronger than that of $Ru(bpy)_3^{2+}$, which provided the advantage of high signal-to-noise ratio for analytical and other related applications. Zou and co-workers [167] reported the 6-aza-2-thiothymine

(ATT)-modified Au NCs, and combined with L-arginine through rigid host guest self-assembly. The formation of rigid host guest self-assembly between the guanidine groups of arginine and Au NCs through hydrogen bond hindered the intramolecular vibration and rotation of ATT, thus reduced the non-radiative transition of excited state and exhibited 70 times enhanced ECL emission in the presence of TPrA.

So far, three types of metal clusters have been applied in ECL biosensing, including Ag NCs [168], Au NCs [169], and Cu NCs [170]. Shen and co-workers [168] prepared bovine serum albumin-stabilized Ag NCs, which exhibited near-infrared ECL peak at 904 nm in aqueous medium. Using CNTs and TiO_2 NPs as accelerators, the ECL intensity of Ag NCs was enhanced by about 16-folds. In a spectrum-resolved triplex-color ECL multiplexing immunoassay, CdSe NCs, CdTe NCs and Ag NCs were used as the ECL probes for determination of carbohydrate antigen 125 (CA125), carbohydrate antigen 19-9 (CA19-9) and cardiac troponin I (cTnI), respectively. The LOD was 0.035 mU/mL for CA125, 0.087 mU/mL for CA19-9, and 0.016 pg/mL for cTnI, respectively. Ju and co-workers [169] recently further modified the glutathione (GSH)-stabilized AuNCs with cysteine, which not only increased the ECL intensity for about 1.5-folds compared with GSH-AuNCs, but also red-shifted the ECL spectrum from 660 to 780 nm due to the limit of the intramolecular motion and nonradiative relaxation of the excited state. Using the dual thiol-stablized AuNPs as ECL probes, a sandwich-type immunosensing of CYFRA 21-1 with good performance was achieved. Lu and co-workers [170] synthesized a near-infrared emissive Cu NCs through a facile one-pot wet chemical reduction method. Compared with other Cu NCs, the prepared Cu NCs showed the maximum intensity at 735 nm with $S_2O_8^{2-}$ as a coreactant, at least 135 nm red-shift. The proposed Cu NCs-based ECL immunosensor for α-fetoprotein exhibited good selectivity and sensitivity. Thus, near-infrared ECL of metal clusters possesses great potential in bioassay application.

8 Summary and perspectives

In summary, as an important branch of ECL luminophores, nanoemitters have achieved great advancements in the last two decades. The advantages of nanoemitters with size- and surface-controlled luminescence, high ECL efficiency, and easily functionalization, make them very suitable as probes or carriers for ECL bioanalysis. Their applications in ECL biosensing and bioimaging include: (1) surface-confined ECL of QDs for low-potential biosensing, (2) monochromatic ECL generation from QDs for multiplexing immunoassay, (3) the LSPR-enhanced ECL generation from CDs for highly sensitive detection, (4) the ERET-enhanced ECL generation from Pdots for biosensing, (5) intramolecular electron transfer strategy for amplifying ECL of Pdots for *in situ* ECL microimaging of membrane protein on single living cells, (6) aggregation-induced enhanced ECL of AIE nanoparticles for biomolecule detection, and (7) nanoemitters complexes for single biomolecule detection.

Nevertheless, nanoemitters still suffer from long-term luminescence instability and heterogeneity of nanoparticles. To meet diverse application demands, it is necessary to develop nanoemitters with higher ECL efficiency, lower excitation potential, and near-infrared emission. In addition to the pursuit of high sensitivity and specificity in biosensing, the development of point-of-care testing (POCT) ECL biosensors for low-resource areas has significant advantages owing to its cost-effectiveness, rapidity, and user-friendliness. Recently, an ECL-incorporated lateral flow immunosensor (ECL-LFI) has been developed for full-range detection of physiological C-reactive protein levels by using $Ru(bpy)_3^{2+}$-labeled gold nanoparticles as probe [171]. For bioimaging, the development of nanoemitters-based super-resolution and *in situ* ECL bioimaging methods can precisely reveal biological processes. Furthermore, wearable ECL sensors provide instant and in-body assessment of personal health status [172,173]. Recently, a flexible and wearable ECL sensor for sweat detection was designed by coupling nanoemitters into gels for non-invasive detection [174]. With the development of high-performance nanoemitters and the profound understanding of the ECL mechanisms, their applications in biosensing and bioimaging will be further expanded.

Acknowledgements This work was supported by the National Natural Science Foundation of China (21804107, 21890741, 21827812), the State Key Laboratory of Analytical Chemistry for Life Science (SKLACLS1807), Taishan Scholars Construction Engineering (tsqn202103112), and the support plan for youth entrepreneurship and technology of colleges and universities in Shandong Province (2021KJ052). The authors also thank Zhuanzhuan Wang and Haijing Guo for literature collection.

Conflict of interest The authors declare no conflict of interest.

1 Bard AJ. *Electrogenerated Chemiluminescence*. New York: Marcel Dekker, 2004
2 Sojic N. *Analytical Electrogenerated Chemiluminescence: From Fundamentals to Bioassays*. London: Royal Society of Chemistry, 2019
3 Richter MM. *Chem Rev*, 2004, 104: 3003–3036
4 Miao W. *Chem Rev*, 2008, 108: 2506–2553
5 Zhou X, Zhu D, Liao Y, Liu W, Liu H, Ma Z, Xing D. *Nat Protoc*, 2014, 9: 1146–1159
6 Wu P, Hou X, Xu JJ, Chen HY. *Chem Rev*, 2014, 114: 11027–11059
7 Liu Z, Qi W, Xu G. *Chem Soc Rev*, 2015, 44: 3117–3142
8 Ma C, Cao Y, Gou X, Zhu JJ. *Anal Chem*, 2020, 92: 431–454
9 Dong J, Lu Y, Xu Y, Chen F, Yang J, Chen Y, Feng J. *Nature*, 2021, 596: 244–249
10 Yang H, Leland JK, Yost D, Massey RJ. *Nat Biotechnol*, 1994, 12: 193–194
11 Hu L, Xu G. *Chem Soc Rev*, 2010, 39: 3275–3304
12 Hesari M, Ding Z. *J Electrochem Soc*, 2016, 163: H3116–H3131
13 Li L, Chen Y, Zhu JJ. *Anal Chem*, 2017, 89: 358–371
14 Ma X, Gao W, Du F, Yuan F, Yu J, Guan Y, Sojic N, Xu G. *Acc*

Chem Res, 2021, 54: 2936–2945
15 Zhang Q, Zhang X, Ma Q. *J Anal Test*, 2020, 4: 92–106
16 Cho KG, Lee JI, Lee S, Hong K, Kang MS, Lee KH. *Adv Funct Mater*, 2020, 30: 1907936
17 Zhou Y, Yin H, Zhao WW, Ai S. *Coord Chem Rev*, 2020, 424: 213519
18 Qi H, Zhang C. *Anal Chem*, 2020, 92: 524–534
19 Zhang S, Liu Y. *Front Chem*, 2021, 8: 626243
20 Chen Y, Zhou S, Li L, Zhu J. *Nano Today*, 2017, 12: 98–115
21 Yang E, Zhang Y, Shen Y. *Anal Chim Acta*, 2021, 1209: 339140
22 Lei J, Ju H. *TrAC Trends Anal Chem*, 2011, 30: 1351–1359
23 Deng S, Ju H. *Analyst*, 2013, 138: 43–61
24 Ju HX, Li JH. *Biochemical Sensors: Fundament and Development*. Singapore: World Scientific, 2021
25 Lei J, Ju H. *Chem Soc Rev*, 2012, 41: 2122–2134
26 Zhang J, Arbault S, Sojic N, Jiang D. *Annu Rev Anal Chem*, 2019, 12: 275–295
27 Ding Z, Quinn BM, Haram SK, Pell LE, Korgel BA, Bard AJ. *Science*, 2002, 296: 1293–1297
28 Zanut A, Palomba F, Rossi Scota M, Rebeccani S, Marcaccio M, Genovese D, Rampazzo E, Valenti G, Paolucci F, Prodi L. *Angew Chem Int Ed*, 2020, 59: 21858–21863
29 Hesari M, Ding Z. *Acc Chem Res*, 2017, 50: 218–230
30 Zhang X, Wang P, Nie Y, Ma Q. *TrAC Trends Anal Chem*, 2021, 143: 116410
31 Fiorani A, Merino JP, Zanut A, Criado A, Valenti G, Prato M, Paolucci F. *Curr Opin Electrochem*, 2019, 16: 66–74
32 Gu Y, Wang J, Shi H, Pan M, Liu B, Fang G, Wang S. *Biosens Bioelectron*, 2019, 128: 129–136
33 Liu F, Du F, Yuan F, Quan S, Guan Y, Xu G. *Curr Opin Electrochem*, 2022, 34: 100981
34 Tan X, Zhang B, Zou G. *J Am Chem Soc*, 2017, 139: 8772–8776
35 Feng Y, Dai C, Lei J, Ju H, Cheng Y. *Anal Chem*, 2016, 88: 845–850
36 Wei X, Zhu MJ, Yan H, Lu C, Xu JJ. *Chem Eur J*, 2019, 25: 12671–12683
37 Feng G, Liu B. *Acc Chem Res*, 2018, 51: 1404–1414
38 Liu X, Cheng L, Lei J, Liu H, Ju H. *Chem Eur J*, 2010, 16: 10764–10770
39 Liu S, Zhang X, Yu Y, Zou G. *Biosens Bioelectron*, 2014, 55: 203–208
40 García de Arquer FP, Talapin DV, Klimov VI, Arakawa Y, Bayer M, Sargent EH. *Science*, 2021, 373: eaaz8541
41 Bard AJ, Ding Z, Myung N. *Struc Bonding*, 2005, 118: 1–57
42 Myung N, Lu X, Johnston KP, Bard AJ. *Nano Lett*, 2004, 4: 183–185
43 Ren T, Xu JZ, Tu YF, Xu S, Zhu JJ. *Electrochem Commun*, 2005, 7: 5–9
44 Myung N, Ding Z, Bard AJ. *Nano Lett*, 2002, 2: 1315–1319
45 Bae Y, Myung N, Bard AJ. *Nano Lett*, 2004, 4: 1153–1161
46 Hesari M, Swanick KN, Lu JS, Whyte R, Wang S, Ding Z. *J Am Chem Soc*, 2015, 137: 11266–11269
47 Myung N, Bae Y, Bard AJ. *Nano Lett*, 2003, 3: 1053–1055
48 Cao Z, Shu Y, Qin H, Su B, Peng X. *ACS Cent Sci*, 2020, 6: 1129–1137
49 Zou G, Ju H. *Anal Chem*, 2004, 76: 6871–6876
50 Jiang H, Ju H. *Chem Commun*, 2007, : 404–406
51 Deng S, Cheng L, Lei J, Cheng Y, Huang Y, Ju H. *Nanoscale*, 2013, 5: 5435–5441
52 Liu X, Zhang Y, Lei J, Xue Y, Cheng L, Ju H. *Anal Chem*, 2010, 82: 7351–7356
53 Lin D, Wu J, Yan F, Deng S, Ju H. *Anal Chem*, 2011, 83: 5214–5221
54 Deng S, Lei J, Huang Y, Yao X, Ding L, Ju H. *Chem Commun*, 2012, 48: 9159
55 Deng S, Lei J, Huang Y, Cheng Y, Ju H. *Anal Chem*, 2013, 85: 5390–5396
56 Han E, Ding L, Lian H, Ju H. *Chem Commun*, 2010, 46: 5446–5448
57 Jiang H, Ju H. *Anal Chem*, 2007, 79: 6690–6696
58 Liu X, Jiang H, Lei J, Ju H. *Anal Chem*, 2007, 79: 8055–8060
59 Liu X, Ju H. *Anal Chem*, 2008, 80: 5377–5382
60 Cheng L, Liu X, Lei J, Ju H. *Anal Chem*, 2010, 82: 3359–3364
61 Dong S, Gao X, Fu L, Jia J, Zou G. *Anal Chem*, 2021, 93: 12250–12256
62 Li Z, Wu S, Zhang B, Fu L, Zou G. *J Phys Chem Lett*, 2019, 10: 5408–5413
63 Fu L, Zhang B, Long X, Fu K, Gao X, Zou G. *Anal Chem*, 2019, 91: 10221–10226
64 Li Z, Wu S, Zou G. *J Electroanal Chem*, 2021, 888: 115173
65 Fu L, Zhang B, Fu K, Gao X, Zou G. *Anal Chem*, 2020, 92: 6144–6149
66 Deiss F, LaFratta CN, Symer M, Blicharz TM, Sojic N, Walt DR. *J Am Chem Soc*, 2009, 131: 6088–6089
67 Guo W, Ding H, Gu C, Liu Y, Jiang X, Su B, Shao Y. *J Am Chem Soc*, 2018, 140: 15904–15915
68 Lv W, Ye H, Yuan Z, Liu X, Chen X, Yang W. *TrAC Trends Anal Chem*, 2020, 123: 115767
69 Zhou J, Nie L, Zhang B, Zou G. *Anal Chem*, 2018, 90: 12361–12365
70 Liu X, Jiang H, Fang Y, Zhao W, Wang N, Zang G. *Anal Chem*, 2015, 87: 9163–9169
71 Jiang Y, Li Q, Xu Y, Bai W, Yang X, Li S, Li Y. *Biosens Bioelectron*, 2022, 201: 113980
72 Zou G, Tan X, Long X, He Y, Miao W. *Anal Chem*, 2017, 89: 13024–13029
73 Derfus AM, Chan WCW, Bhatia SN. *Nano Lett*, 2004, 4: 11–18
74 Lovrić J, Cho SJ, Winnik FM, Maysinger D. *Chem Biol*, 2005, 12: 1227–1234
75 Đorđević L, Arcudi F, Cacioppo M, Prato M. *Nat Nanotechnol*, 2022, 17: 112–130
76 Miao S, Liang K, Zhu J, Yang B, Zhao D, Kong B. *Nano Today*, 2020, 33: 100879
77 Baker SN, Baker GA. *Angew Chem Int Ed*, 2010, 49: 6726–6744
78 Liu J, Li R, Yang B. *ACS Cent Sci*, 2020, 6: 2179–2195
79 Arcudi F, Đorđević L, Prato M. *Acc Chem Res*, 2019, 52: 2070–2079
80 Semeniuk M, Yi Z, Poursorkhabi V, Tjong J, Jaffer S, Lu ZH, Sain M. *ACS Nano*, 2019, 13: 6224–6255
81 Hu C, Li M, Qiu J, Sun YP. *Chem Soc Rev*, 2019, 48: 2315–2337
82 Li H, Yan X, Kong D, Jin R, Sun C, Du D, Lin Y, Lu G. *Nanoscale Horiz*, 2020, 5: 218–234
83 Chung YJ, Kim J, Park CB. *ACS Nano*, 2020, 14: 6470–6497
84 Dhenadhayalan N, Lin KC, Saleh TA. *Small*, 2020, 16: 1905767
85 Chen Y, Cao Y, Ma C, Zhu JJ. *Mater Chem Front*, 2020, 4: 369–385
86 Zheng L, Chi Y, Dong Y, Lin J, Wang B. *J Am Chem Soc*, 2009, 131: 4564–4565
87 Qin Y, Liu N, Li H, Sun Y, Hu L, Zhao S, Han D, Liu Y, Kang Z, Niu L. *J Phys Chem C*, 2017, 121: 27546–27554
88 Zhu H, Wang X, Li Y, Wang Z, Yang F, Yang X. *Chem Commun*, 2009, 34: 5118–5120
89 Zhou J, Booker C, Li R, Sun X, Sham TK, Ding Z. *Chem Phys Lett*, 2010, 493: 296–298
90 Li LL, Ji J, Fei R, Wang CZ, Lu Q, Zhang JR, Jiang LP, Zhu JJ. *Adv Funct Mater*, 2012, 22: 2971–2979
91 Dong Y, Chen C, Lin J, Zhou N, Chi Y, Chen G. *Carbon*, 2013, 56: 12–17
92 Zheng Y, Lin J, Xie L, Zhuo Y, Tang H, Wang K, Liu J. *Front Chem*, 2021, 9: 688358
93 Arcudi F, Đorđević L, Rebeccani S, Cacioppo M, Zanut A, Valenti G, Paolucci F, Prato M. *Adv Sci*, 2021, 8: 2100125
94 Zhang R, Adsetts JR, Nie Y, Sun X, Ding Z. *Carbon*, 2018, 129: 45–53
95 Wang X, Zhang M, Huo X, Zhao W, Kang B, Xu JJ, Chen H. *Nanoscale Adv*, 2019, 1: 1965–1969
96 Carrara S, Arcudi F, Prato M, De Cola L. *Angew Chem Int Ed*, 2017, 56: 4757–4761
97 Xiong H, Huang Z, Lin Q, Yang B, Yan F, Liu B, Chen H, Kong J. *Anal Chem*, 2022, 94: 837–846
98 Zhu S, Wang L, Zhou N, Zhao X, Song Y, Maharjan S, Zhang J, Lu L, Wang H, Yang B. *Chem Commun*, 2014, 50: 13845–13848
99 Chen A, Liang W, Wang H, Zhuo Y, Chai Y, Yuan R. *Anal Chem*, 2020, 92: 1379–1385
100 Cai XL, Zheng B, Zhou Y, Younis MR, Wang FB, Zhang WM, Zhou YG, Xia XH. *Chem Sci*, 2018, 9: 6080–6084

101 Qin D, Jiang X, Mo G, Feng J, Yu C, Deng B. *ACS Sens*, 2019, 4: 504–512
102 Wu C, Chiu DT. *Angew Chem Int Ed*, 2013, 52: 3086–3109
103 Yu J, Rong Y, Kuo CT, Zhou XH, Chiu DT. *Anal Chem*, 2017, 89: 42–56
104 MacFarlane LR, Shaikh H, Garcia-Hernandez JD, Vespa M, Fukui T, Manners I. *Nat Rev Mater*, 2021, 6: 7–26
105 Chang YL, Palacios RE, Fan FRF, Bard AJ, Barbara PF. *J Am Chem Soc*, 2008, 130: 8906–8907
106 Nepomnyashchii AB, Ono RJ, Lyons DM, Sessler JL, Bielawski CW, Bard AJ. *J Phys Chem Lett*, 2012, 3: 2035–2038
107 Dai R, Wu F, Xu H, Chi Y. *ACS Appl Mater Interfaces*, 2015, 7: 15160–15167
108 Wu F, Feng Y, Chi Y. *J Electroanal Chem*, 2016, 779: 47–54
109 Luo Y, Zhao B, Zhang B, Lan Y, Chen L, Zhang Y, Bao Y, Niu L. *Analyst*, 2022, 147: 2442–2451
110 Lu Q, Zhang J, Wu Y, Chen S. *RSC Adv*, 2015, 5: 63650–63654
111 Chen H, Lu Q, Liao J, Yuan R, Chen S. *Chem Commun*, 2016, 52: 7276–7279
112 Wang Z, Guo H, Luo Z, Duan Y, Feng Y. *Anal Chem*, 2022, 94: 5615–5623
113 Feng Y, Sun F, Wang N, Lei J, Ju H. *Anal Chem*, 2017, 89: 7659–7666
114 Zhang N, Zhao ZY, Gao H, Yu Y, Pan JB, Chen HY, Xu JJ. *J Electroanal Chem*, 2021, 900: 115743
115 Luo JH, Li Q, Chen SH, Yuan R. *ACS Appl Mater Interfaces*, 2019, 11: 27363–27370
116 Feng Y, Wang N, Ju H. *Anal Chem*, 2018, 90: 1202–1208
117 Wang N, Feng Y, Wang Y, Ju H, Yan F. *Anal Chem*, 2018, 90: 7708–7714
118 Ackerman CM, Myhrvold C, Thakku SG, Freije CA, Metsky HC, Yang DK, Ye SH, Boehm CK, Kosoko-Thoroddsen TSF, Kehe J, Nguyen TG, Carter A, Kulesa A, Barnes JR, Dugan VG, Hung DT, Blainey PC, Sabeti PC. *Nature*, 2020, 582: 277–282
119 Li M, Yin F, Song L, Mao X, Li F, Fan C, Zuo X, Xia Q. *Chem Rev*, 2021, 121: 10469–10558
120 Wang N, Chen L, Chen W, Ju H. *Anal Chem*, 2021, 93: 5327–5333
121 Wang N, Wang Z, Chen L, Chen W, Quan Y, Cheng Y, Ju H. *Chem Sci*, 2019, 10: 6815–6820
122 Valenti G, Scarabino S, Goudeau B, Lesch A, Jović M, Villani E, Sentic M, Rapino S, Arbault S, Paolucci F, Sojic N. *J Am Chem Soc*, 2017, 139: 16830–16837
123 Voci S, Goudeau B, Valenti G, Lesch A, Jović M, Rapino S, Paolucci F, Arbault S, Sojic N. *J Am Chem Soc*, 2018, 140: 14753–14760
124 Wang N, Gao H, Li Y, Li G, Chen W, Jin Z, Lei J, Wei Q, Ju H. *Angew Chem Int Ed*, 2021, 60: 197–201
125 Wang N, Ao H, Xiao W, Chen W, Li G, Wu J, Ju H. *Biosens Bioelectron*, 2022, 201: 113959
126 Mei J, Leung NLC, Kwok RTK, Lam JWY, Tang BZ. *Chem Rev*, 2015, 115: 11718–11940
127 Luo J, Xie Z, Lam JWY, Cheng L, Tang BZ, Chen H, Qiu C, Kwok HS, Zhan X, Liu Y, Zhu D. *Chem Commun*, 2001, : 1740–1741
128 Wang X, Gao Z, Zhu J, Gao Z, Wang F. *Polym Chem*, 2016, 7: 5217–5220
129 Carrara S, Aliprandi A, Hogan CF, De Cola L. *J Am Chem Soc*, 2017, 139: 14605–14610
130 Li K, Zhu Z, Cai P, Liu R, Tomczak N, Ding D, Liu J, Qin W, Zhao Z, Hu Y, Chen X, Tang BZ, Liu B. *Chem Mater*, 2013, 25: 4181–4187
131 Chen S, Wang H, Hong Y, Tang BZ. *Mater Horiz*, 2016, 3: 283–293
132 Liu H, Wang L, Gao H, Qi H, Gao Q, Zhang C. *ACS Appl Mater Interfaces*, 2017, 9: 44324–44331
133 Jiang MH, Li SK, Zhong X, Liang WB, Chai YQ, Zhuo Y, Yuan R. *Anal Chem*, 2019, 91: 3710–3716
134 Liu JL, Zhang JQ, Tang ZL, Zhuo Y, Chai YQ, Yuan R. *Chem Sci*, 2019, 10: 4497–4501
135 Guo J, Feng W, Du P, Zhang R, Liu J, Liu Y, Wang Z, Lu X. *Anal Chem*, 2020, 92: 14838–14845
136 Lv W, Yang Q, Li Q, Li H, Li F. *Anal Chem*, 2020, 92: 11747–11754
137 Wang X, Liu H, Jiang J, Qian M, Qi H, Gao Q, Zhang C. *Anal Chem*, 2022, 94: 5441–5449
138 Jin XH, Price MB, Finnegan JR, Boott CE, Richter JM, Rao A, Menke SM, Friend RH, Whittell GR, Manners I. *Science*, 2018, 360: 897–900
139 Wu Z, Sun C, Dong S, Jiang XF, Wu S, Wu H, Yip HL, Huang F, Cao Y. *J Am Chem Soc*, 2016, 138: 2004–2013
140 Sun F, Wang Z, Feng Y, Cheng Y, Ju H, Quan Y. *Biosens Bioelectron*, 2018, 100: 28–34
141 Ji SY, Zhao W, Gao H, Pan JB, Xu CH, Quan YW, Xu JJ, Chen HY. *iScience*, 2020, 23: 100774
142 Wang Z, Feng Y, Wang N, Cheng Y, Quan Y, Ju H. *J Phys Chem Lett*, 2018, 9: 5296–5302
143 Zhang N, Gao H, Jia YL, Pan JB, Luo XL, Chen HY, Xu JJ. *Anal Chem*, 2021, 93: 6857–6864
144 Wang Z, Pan J, Li Q, Zhou Y, Yang S, Xu J, Hua D. *Adv Funct Mater*, 2020, 30: 2000220
145 Valenti G, Rampazzo E, Bonacchi S, Petrizza L, Marcaccio M, Montalti M, Prodi L, Paolucci F. *J Am Chem Soc*, 2016, 138: 15935–15942
146 Yang X, Yuan R, Chai Y, Zhuo Y, Mao L, Yuan S. *Biosens Bioelectron*, 2010, 25: 1851–1855
147 Qi W, Wu D, Zhao J, Liu Z, Zhang W, Zhang L, Xu G. *Anal Chem*, 2013, 85: 3207–3212
148 Lian S, Huang Z, Lin Z, Chen X, Oyama M, Chen X. *Sens Actuat B-Chem*, 2016, 236: 614–620
149 Su Y, Lai W, Liang Y, Zhang C. *Anal Chim Acta*, 2022, 1206: 339789
150 Liang W, Zhuo Y, Xiong C, Zheng Y, Chai Y, Yuan R. *Biosens Bioelectron*, 2017, 94: 568–574
151 Shan Y, Xu JJ, Chen HY. *Nanoscale*, 2011, 3: 2916–2923
152 Liu Y, Zhang H, Li B, Liu J, Jiang D, Liu B, Sojic N. *J Am Chem Soc*, 2021, 143: 17910–17914
153 Jin Z, Zhu X, Wang N, Li Y, Ju H, Lei J. *Angew Chem Int Ed*, 2020, 59: 10446–10450
154 Liu J, Huang J, Zhang L, Lei J. *Chem Soc Rev*, 2021, 50: 1188–1218
155 Wang Y, Zhang Y, Sha H, Xiong X, Jia N. *ACS Appl Mater Interfaces*, 2019, 11: 36299–36306
156 Zhou Y, He J, Zhang C, Li J, Fu X, Mao W, Li W, Yu C. *ACS Appl Mater Interfaces*, 2020, 12: 338–346
157 Huang W, Hu GB, Yao LY, Yang Y, Liang WB, Yuan R, Xiao DR. *Anal Chem*, 2020, 92: 3380–3387
158 Wang Y, Zhao G, Chi H, Yang S, Niu Q, Wu D, Cao W, Li T, Ma H, Wei Q. *J Am Chem Soc*, 2021, 143: 504–512
159 Wang C, Li Z, Ju H. *Anal Chem*, 2021, 93: 14878–14884
160 Yang X, Yu YQ, Peng LZ, Lei YM, Chai YQ, Yuan R, Zhuo Y. *Anal Chem*, 2018, 90: 3995–4002
161 Nie Y, Tao X, Zhang H, Chai YQ, Yuan R. *Anal Chem*, 2021, 93: 3445–3451
162 Xu Y, Yin XB, He XW, Zhang YK. *Biosens Bioelectron*, 2015, 68: 197–203
163 Zhu D, Zhang Y, Bao S, Wang N, Yu S, Luo R, Ma J, Ju H, Lei J. *J Am Chem Soc*, 2021, 143: 3049–3053
164 Zhang JL, Yang Y, Liang WB, Yao LY, Yuan R, Xiao DR. *Anal Chem*, 2021, 93: 3258–3265
165 Luo R, Lv H, Liao Q, Wang N, Yang J, Li Y, Xi K, Wu X, Ju H, Lei J. *Nat Commun*, 2021, 12: 6808
166 Chen S, Ma H, Padelford JW, Qinchen W, Yu W, Wang S, Zhu M, Wang G. *J Am Chem Soc*, 2019, 141: 9603–9609
167 Yang L, Zhang B, Fu L, Fu K, Zou G. *Angew Chem Int Ed*, 2019, 58: 6901–6905
168 Yu L, Li M, Kang Q, Fu L, Zou G, Shen D. *Biosens Bioelectron*, 2021, 176: 112934
169 Jia H, Yang L, Dong X, Zhou L, Wei Q, Ju H. *Anal Chem*, 2022, 94: 2313–2320
170 Lv H, Zhang R, Cong S, Guo J, Shao M, Liu W, Zhang L, Lu X. *Anal Chem*, 2022, 94: 4538–4546
171 Hong D, Kim K, Jo EJ, Kim MG. *Anal Chem*, 2021, 93: 7925–7932
172 Kwon JH, Kim YM, Moon HC. *ACS Nano*, 2021, 15: 15132–15141
173 Kwon DK, Myoung JM. *ACS Nano*, 2020, 14: 8716–8723
174 Chen MM, Cheng SB, Ji K, Gao J, Liu YL, Wen W, Zhang X, Wang S, Huang WH. *Chem Sci*, 2019, 10: 6295–6303